DTIC FILE COPY

AD-A227 643

December 1989 Thesis/Dissertation

# Cross-Equatorial Influences of a South American Cold Surge on the Development of Two Eastern North Pacific Tropical Cyclones

Vicki Anne Millier

AFIT Student at: Texas A&M University

AFIT/CI/CIA - 90-102

AFIT/CI
Wright-Patterson AFB OH 45433

Approved for Public Release IAW AFR 190-1
Distribution Unlimited
ERNEST A. HAYGOOD, 1st Lt, USAF
Executive Officer, Civilian Institution Programs

DTIC
ELECTE
OCT 23 1990
S B D



UNCLASSIFIED

## GENERAL INSTRUCTIONS FOR COMPLETING SF 298

The Report Documentation Page (RDP) is used in announcing and cataloging reports. It is important that this information be consistent with the rest of the report, particularly the cover and title page. Instructions for filling in each block of the form follow. It is important to **stay within the lines to meet optical scanning requirements.**

**Block 1.** Agency Use Only (Leave Blank)

**Block 2.** Report Date. Full publication date including day, month, and year, if available (e.g. 1 Jan 88). Must cite at least the year.

**Block 3.** Type of Report and Dates Covered. State whether report is interim, final, etc. If applicable, enter inclusive report dates (e.g. 10 Jun 87 - 30 Jun 88).

**Block 4.** Title and Subtitle. A title is taken from the part of the report that provides the most meaningful and complete information. When a report is prepared in more than one volume, repeat the primary title, add volume number, and include subtitle for the specific volume. On classified documents enter the title classification in parentheses.

**Block 5.** Funding Numbers. To include contract and grant numbers; may include program element number(s), project number(s), task number(s), and work unit number(s). Use the following labels:

| | | | |
|---|---|---|---|
| **C** | - Contract | **PR** | - Project |
| **G** | - Grant | **TA** | - Task |
| **PE** | - Program Element | **WU** | - Work Unit Accession No. |

**Block 6.** Author(s). Name(s) of person(s) responsible for writing the report, performing the research, or credited with the content of the report. If editor or compiler, this should follow the name(s).

**Block 7.** Performing Organization Name(s) and Address(es). Self-explanatory.

**Block 8.** Performing Organization Report Number. Enter the unique alphanumeric report number(s) assigned by the organization performing the report.

**Block 9.** Sponsoring/Monitoring Agency Names(s) and Address(es). Self-explanatory.

**Block 10.** Sponsoring/Monitoring Agency. Report Number. (If known)

**Block 11.** Supplementary Notes. Enter information not included elsewhere such as: Prepared in cooperation with...; Trans. of ..., To be published in .... When a report is revised, include a statement whether the new report supersedes or supplements the older report.

**Block 12a.** Distribution/Availablity Statement. Denote public availability or limitation. Cite any availability to the public. Enter additional limitations or special markings in all capitals (e.g. NOFORN, REL, ITAR)

| | |
|---|---|
| **DOD** | - See DoDD 5230.24, "Distribution Statements on Technical Documents." |
| **DOE** | - See authorities |
| **NASA** | - See Handbook NHB 2200.2. |
| **NTIS** | - Leave blank. |

**Block 12b.** Distribution Code.

| | |
|---|---|
| **DOD** | - DOD - Leave blank |
| **DOE** | - DOE - Enter DOE distribution categories from the Standard Distribution for Unclassified Scientific and Technical Reports |
| **NASA** | - NASA - Leave blank |
| **NTIS** | - NTIS - Leave blank. |

**Block 13.** Abstract. Include a brief (Maximum 200 words) factual summary of the most significant information contained in the report.

**Block 14.** Subject Terms. Keywords or phrases identifying major subjects in the report.

**Block 15.** Number of Pages. Enter the total number of pages.

**Block 16.** Price Code. Enter appropriate price code (NTIS only).

**Blocks 17. - 19.** Security Classifications. Self-explanatory. Enter U.S. Security Classification in accordance with U.S. Security Regulations (i.e., UNCLASSIFIED). If form contains classified information, stamp classification on the top and bottom of the page.

**Block 20.** Limitation of Abstract. This block must be completed to assign a limitation to the abstract. Enter either UL (unlimited) or SAR (same as report). An entry in this block is necessary if the abstract is to be limited. If blank, the abstract is assumed to be unlimited.

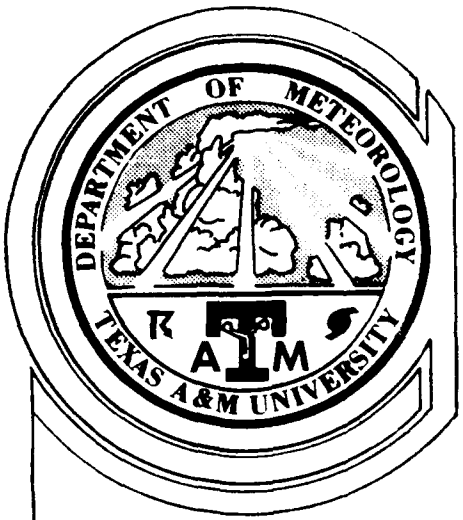


# TEXAS A&M UNIVERSITY

DEPARTMENT OF
METEOROLOGY

## CROSS-EQUATORIAL INFLUENCES OF A SOUTH AMERICAN COLD SURGE ON THE DEVELOPMENT OF TWO EASTERN NORTH PACIFIC TROPICAL CYCLONES

A Thesis

by

VICKI ANNE MILLIER

Submitted to the Office of Graduate Studies of
Texas A&M University
in partial fulfillment of the requirements for the degree of

MASTER OF SCIENCE

December 1989

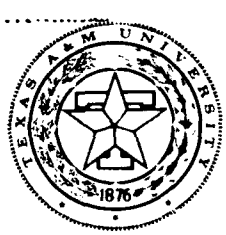


90

# CROSS-EQUATORIAL INFLUENCES OF A SOUTH AMERICAN COLD SURGE ON THE DEVELOPMENT OF TWO EASTERN NORTH PACIFIC TROPICAL CYCLONES

A Thesis

by

VICKI ANNE MILLIER

Submitted to the Office of Graduate Studies of
Texas A&M University
in partial fulfillment of the requirements for the degree of

MASTER OF SCIENCE

December 1989

Major Subject: Meteorology

prior to tropical cyclone genesis. This strong vertical overturning appears to have provided the upper level outflow mechanism necessary for tropical cyclone genesis.

Global geopotential height studies indicate that both the strong amplification of the Southern hemisphere wave and the strengthening of the Hadley Cell circulation coincided with the downstream passage of energy over South America, and that this downstream propagation originated somewhere in the West Pacific at more than three days before it advanced over South America.

DTIC COPY INSPECTED 6

Accession For
NTIS GRA&I ☑
DTIC TAB ☐
Unannounced ☐
Justification
By
Distribution/
Availability Codes
Dist | Avail and/or Special
A-1

# ACKNOWLEDGEMENTS

My sojourn through academia and research has left me indelibly marked and grateful to a variety of people. First and foremost I would like to express my gratitude to my chairman Dr. Steven W. Lyons, who challenged and guided me through the world of research methodology, who despite his busy schedule took many hours out to help me understand and interpret my results. His good nature and understanding tolerance were appreciated more than I can express. I would also like to thank my other committee members Dr. Dušan Djurič, Dr. John Klink, and Dr. David Brooks for their constructive criticism and valuable insight.

A special thank you is extended to my friends both near and far; for their patience, encouragement, joy at my small successes, and for all the little things that each one contributed that together add up to so much. I would especially like to thank Mark Ivy whose friendship has touched and enriched me these last two years, whose moral support and encouragement are unending, and who magnanimously put up with my many discourses on unintelligible topics.

And finally I would like to thank Charlie, my love.

# DEDICATION

In memory of my parents

for their gift of life and love

# LIST OF SYMBOLS

| | |
|---|---|
| $\theta, \lambda$ | latitude and longitude respectively |
| $u, v$ | zonal and meridional winds respectively |
| $w$ | vertical velocity |
| $\phi$ | geopotential height |
| $\zeta$ | vorticity |
| $D$ | divergence |
| $\chi$ | velocity potential |
| $f$ | Coriolis parameter |
| $\beta$ | $\partial f/\partial y$, Rossby Parameter |
| gpm | geopotential meters |
| $a_o$ | mean geopotential height |
| $C_n$ | wave amplitude coifficient |
| $a_n$ | cosine coifficient in the series |
| $b_n$ | sine coifficient in the series |
| $n$ | wave number |
| $I$ | number of grid intervals |
| $\phi_n$ | phase between the wave maximum and the origin |

# TABLE OF CONTENTS

# CHAPTER I

# INTRODUCTION

Of all natural disasters tropical cyclones are among the most severe. Approximately 80 tropical cyclones occur over the earth each year and are responsible for the loss of hundreds of lives and millions of dollars worth of damage. While tropical cyclones are very destructive, they are also beneficial. Tropical cyclones provide needed rainfall to arid regions, as well as help maintain the moisture and energy budgets of the earth.

Considerable research has been conducted on the environmental conditions necessary for tropical cyclone genesis. Primarily this research has centered around the climatic requirements necessary for development. Gray (1975) established six genesis parameters which are useful in identifying regions and seasons of tropical cyclone genesis. Unfortunately, while these parameters are very useful in a climatological sense, it is still difficult to predict the specific location and time of tropical cyclone formation. One approach to understanding this problem is to identify a feature or a synoptic situation that is common in regions of tropical cyclone genesis and conduct an intense diagnostic study to determine how this feature or synoptic situation relates to the development of tropical cyclones. Love (1982) found that about 75% of the 74 genesis events studied (in longitudes 100° E to 180° E) are associated with an equatorward surge of cold air in the opposing hemisphere. Thus, indicating that

---

The style used is similar to that of the *Monthly Weather Review*.

there appears to be a strong correlation between tropical cyclone genesis and cold surges.

This thesis is a case study of such an event. In late May 1979 a severe cold front passed over South America. On the mornings of 31 May and 1 June four states in Brazil experienced the worst freeze since 1975. Simultaneously, two tropical cyclones developed off the west coast of Central America. The only time in recorded history that two cyclones have developed on the same day in May in this region. The objective of this research is to diagnose this case study to determine if the unusually strong South American cold surge was influential in the development of the two eastern North Pacific tropical cyclones.

# CHAPTER II

# PREVIOUS WORK

Tropical meteorology research was limited before the 1960's due to the lack of satellite imagery and to the sparse amount of upper air observations. However, some major breakthroughs occurred during this period. Palmen (1948) determined that a sea surface temperature of at least 26.5°C was necessary for tropical cyclone genesis. A number of authors (Riehl, 1948; Alaka, 1958; Ramage, 1959) advanced the idea a priori, that for a tropical cyclone to form some type of upper tropospheric outflow is initially established over the disturbance which enhances or triggers low-level convergence.

This theory was refuted in 1964 when the CISK (Conditional Instability of the Second Kind) theory was developed; it explained mechanisms involved in the evolution of tropical disturbances into tropical cyclones. The unstable growth found in tropical cyclones was the result of cooperative interaction between cumulus convection and a large-scale perturbation. The cumulus supplies the heat necessary to drive the large-scale disturbance and produces the moisture convergence needed to drive the cumulus convection (Charney and Eliassen, 1964). Therefore, contrary to the earlier theory, the CISK theory states that the low-level convergence associated with the perturbation must be present before substantial divergent outflow in the upper troposphere can be established.

Gray (1968) conducted the first global study on the origin of tropical disturbances and storms. He compiled over 1500 observations on 300 cases of tropical

disturbances for four tropical genesis areas. He reaffirmed previous findings that tropical cyclones rarely form within 4° latitude of the equator, and concluded this was due to the low magnitude of the Coriolis parameter. He also found that large values of positive vorticity in the low levels, and weak vertical wind shear through the tropopause play crucial roles in tropical cyclone genesis. Gray (1975) later added two additional parameters related to tropical genesis; namely, high mid-level relative humidity and a strong vertical equivalent potential temperature gradient.

McBride and Zehr (1981) examined the thermodynamic and dynamic fields surrounding developing and non-developing tropical weather systems in the northwest Pacific and the northwest Atlantic. They found little difference in the thermodynamic fields between the two types of systems; however, they found large differences in the dynamic fields. They discovered that pre-typhoon and pre-hurricane systems were located in regions of high values of low-level vorticity. The low-level vorticity in the vicinity of a developing cloud cluster was approximately twice as large as observed with non-developing cloud clusters. McBride and Zehr also determined that cyclone genesis occurred under conditions of zero vertical wind shear near the system center and that large-scale cyclonic flow surrounded the center of the incipient disturbance. They concluded that while the thermodynamic features are relatively stable throughout the season in the tropics, the dynamic features (wind field, vorticity field) change on a daily basis. Therefore, while the thermodynamic conditions may all be present, genesis would not occur until favorable dynamic features are present. Thus, a favorable large scale kinematic field appeared to be the determining factor for genesis.

It then became clear that in order to understand tropical cyclone genesis it was first necessary to understand the kinematic processes capable of producing favorable conditions for genesis (i.e. low-level cyclonic flow, high low-level vorticity, weak vertical wind shear). Love (1985a) studied two cases of cross-equatorial influences of winter hemisphere cold surges on the summer hemisphere tropics. He found that a subtropical cold surge in the winter hemisphere is one mechanism capable of producing the favorable large-scale kinematic environment necessary for summer hemisphere tropical cyclone genesis. As the cold core subtropical high pressure system moves equatorward, it induces an equatorial pressure rise and establishes a west-east pressure gradient at low-latitudes in the opposite hemisphere. This leads to enhanced cross-equatorial flow and an increase in low-level westerly flow in the low-latitudes of the summer hemisphere, thereby increasing the low-level vorticity and cyclonic flow required for tropical cyclone genesis.

In a companion paper Love (1985b) used a rawinsonde composite technique to examine the large-scale flow prior to cyclone development. Again he discovered that tropical cyclone development is influenced by events in the winter hemisphere. He found that prior to cyclone genesis there was an intensification of the winter hemisphere Hadley Cell. Additionally, he noted a corresponding increase in the strength of the westerlies equatorward of the precyclone disturbance and an increase in the strength of the upper level equatorial easterlies. Furthermore, in a survey of 74 genesis events, he found that 75% appeared to be associated with a cold surge in the opposing hemisphere (Love, 1982).

Although case studies have been conducted previously on the same cold surge event that I have researched, no studies have been conducted linking the cold surge to tropical cyclone genesis in the eastern North Pacific. Fortune and Kousky (1983) conducted a study of the May 1979 cold surge event and found that the severe cold surge was due to a phase interaction between a short and long wave over South America. Chu (1986) also studied this cold surge event; he investigated the kinematic features of the tropospheric circulation associated with the cold surge. His study indicated upper tropospheric divergence over the area of cyclone genesis and strong upper-level convergence associated with the intense sub-tropical ridge behind the front, indicating a strong inter-hemispheric Hadley Cell circulation. Based on Chu's work, it appears there is a cross equatorial interaction between the region of tropical cyclone development and the cold surge.

# CHAPTER III

# DOMAIN AND DATA DESCRIPTION

## III.1 FGGE Data

The primary data source used for this study is a European Centre for Medium Range Weather Forecast (ECMWF) First GARP Global Experiment (FGGE) III-b data set for the period 26 May–2 June 1979. A subset of the full FGGE data set was used in this study. It includes twice daily data (00Z, 12Z) and contains four variables (temperature, geopotential height, u-wind and v-wind components) at six levels (1000 mb, 850 mb, 700 mb, 500 mb, 300 mb, 200 mb). The data set is global in domain; however, the primary region of interest for this study was 150°W to 5°W, 30°N to 60°S (Fig. 1) .

The First GARP Global Experiment (FGGE) was conducted in 1979 (Bengtsson et al., 1982). It was a worldwide effort to compile the best data set ever to be used for meteorological research. The initial data for the FGGE experiment were compiled by Bengtsson et al. from a number of sources: land based radiosonde and surface observations, ship and aircraft observations, satellite derived winds, and buoy reports. The data were compiled and sorted. Erroneous data were discarded and suspicious data were rechecked. A three-dimensional optimal multivariate interpolation technique was then used to align the data onto a grid covering the earth at 1.875° grid intervals. This technique assigns weights to observations (determined by the distribution and error characteristic of the data), interpolates the weights and

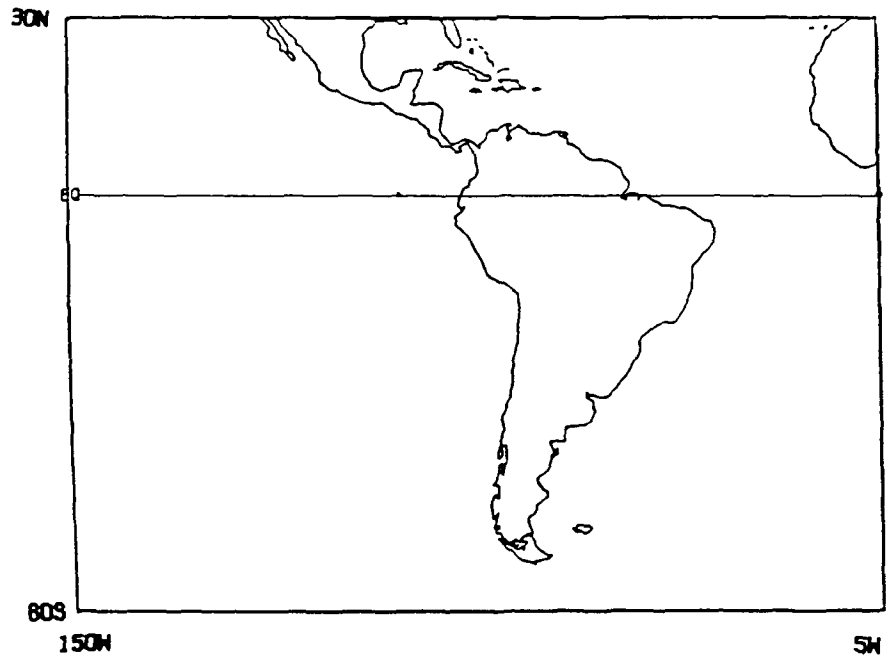


Figure 1. Spatial domain of this study

best fits the data to the grid. A 15 level model extending from 1000 mb to 10 mb was then used for the dynamical assimilation.

The resolution of this data set is 1.875°, or approximately 113 km at the equator. However, over the region of study observations are sparse and data resolution is much coarser than 113 km. Since the size of the tropical cyclones is at about 400 km, it is unreasonable to expect this data set to resolve the two tropical cyclones under investigation in this study. And in fact the objective of this research is not to resolve these vorticies, but to analyze the large scale circulation and environment to determine if an inter-hemispheric interaction was influential in the development of the tropical cyclones.

Although the FGGE data set is the best meteorological data set ever compiled, there are many regions of the world (primarily over oceanic and remote mountainous regions) where the initial observations were sparse, and therefore the data set is likely to be less accurate.

The FGGE wind data is used extensively in this study; the data are computed from available wind observations and satellite derived winds. Satellite winds are computed at half hour intervals from the cloud track analyses taken from the geostationary satellite imagery. However, it is difficult to determine the cloud levels over oceanic regions where observations are sparse, and some accuracy is lost in estimating these levels. In the tropics, where fair weather cumulus and cirrus from thunderstorm blowoffs are the most common cloud types, the most accurate satellite wind data are at the 850 mb and 200 mb levels. Very little information is available at the mid levels; wind data must be interpolated from other levels to obtain the mid-level winds. This is another source of error. Fortunately, the levels of interest in the tropics are the low and high levels, so this error has little impact on this research. An additional source of error associated with the wind field is the bias the wind interpolation model puts on the rotational wind component. Due to the reduced magnitude of the Coriolis parameter in the tropics, the rotational wind is not as accurate a representation of the total wind field as regions in the higher latitudes. Therefore, the suppression of the divergent wind by the wind models can lead to errors in the FGGE wind data. In regions of strong divergence, such as in the upper levels over convectively active regions, it is impossible for the wind models to suppress the divergent wind, therefore,

it is likely that the FGGE wind data in the tropics are most accurate in these strongly convective areas.

Despite the number of small errors that affect FGGE wind data, the data set appears to be very reliable. Comparisons between the FGGE wind data and OLR data (which are generally considered to be very accurate, see next section) reveal that field coincide very well. The maximum regions of cloudiness line up very well with regions of upper level anticyclones. While certainly every wind vector may be not be exact, the large-scale circulation features do appear to be correct. Comparison with OLR works well at 200 mb, but at lower levels synoptic features may be obscured by higher clouds. However, synoptic features at the 850 mb level can be followed from map to map and are very consistent. This consistency implies that the large-scale low-level features are also reasonably correct.

### III.2 OLR Data

OLR (outgoing longwave radiation) data from the National Oceanographic and Atmospheric Administration (NOAA) /National Environmental Satellite Service (NESS) were also used in this study for the period 26 May to 2 June 1979. These IR data (10.5-12.5 $\mu$m) are compiled from data assimilated by the NOAA 7 polar orbiting satellite. The data are twice daily with morning and evening equatorial crossing time varying from 0230 to 0900 LST (northbound) and 1430 to 2100 LST (southbound). The original 8 km resolution data are spatially averaged, digitized and aligned onto 2.5° longitude-latitude grids. The process is described in detail by Gruber and Winston (1978) and Gruber and Kruger (1984).

OLR is used to measure cloudiness over a region. Low OLR values of less than approximately 240 $W/m^2$ in the tropics are generally associated with cloudy, convectively active regions. High OLR values of greater than approximately 260 $W/m^2$ are regions associated with clear to partly cloudy conditions. Since data are compiled from the amount of outgoing radiation at the top of the atmosphere, OLR data are most useful in determining the amount of high cloudiness. One disadvantage of OLR data is in regions of extensive high clouds it is impossible to get an indication of the amount of mid or low level clouds below. Despite this shortcoming, OLR data sets are considered to be very accurate. This is primarily because each OLR value represents an average of the 8 km pixels within its 2.5° domain.

# CHAPTER IV

# SCENARIO OF THE COLD SURGE AND TROPICAL CYCLONE GENESIS EVENTS

Two very unusual weather events occurred in late May 1979: an unusually strong cold front passed over South America and two tropical cyclones developed nearly simultaneously in the eastern North Pacific. Before investigating the interaction between these two systems, it is useful to examine the development of the cold surge and the tropical cyclones separately.

## IV.1 The Cold Surge

It is not unusual in late fall for cold fronts to pass over South America. However, the cold front that passed over South America in late May 1979 was hardly typical. The front was extremely intense. In the first 36 hours of its life the cold front advanced northeast over South America at a rate of 700 km per day (Fortune and Kousky, 1983). The freeze associated with the cold air behind the front extended as far north as southern Brazil and was the worst cold surge experienced in Brazil since 1975. Fortune and Kousky (1983) studied this cold front (Fig. 2) and found that the strong cold surge was the result of the superposition of a shortwave trough on a longwave trough as it approached its peak development over South America.

The 850 mb temperature reveals the intense strength of the front as it passed over South America. These charts were compiled using the FGGE temperature data for the period 27 May–1 June. At 0000 UTC 27 May (Fig. 3) a cold trough is located

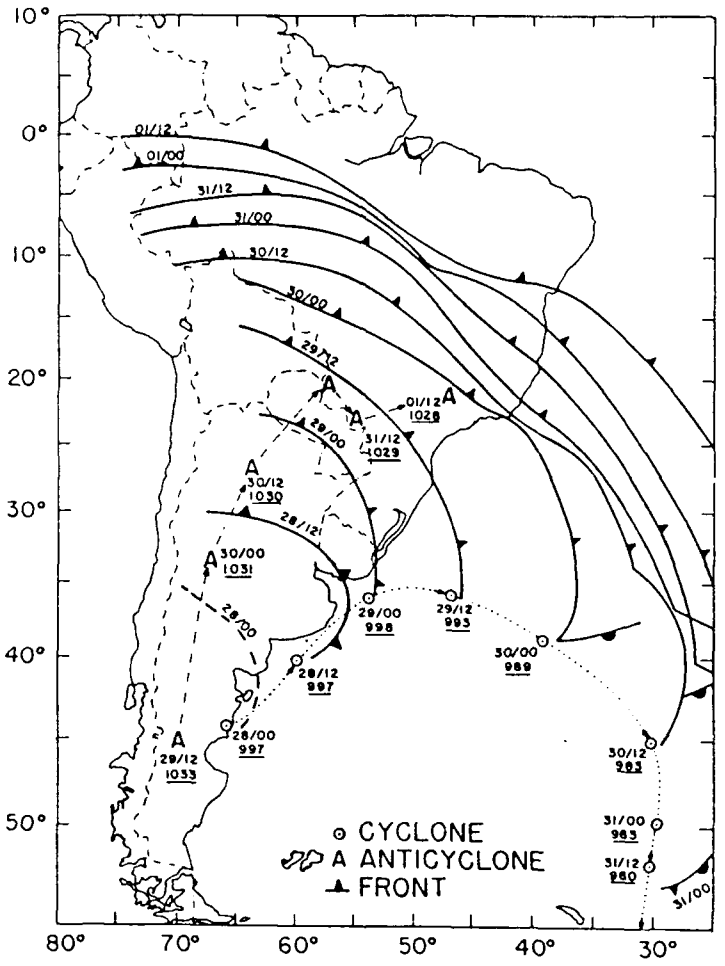


Figure 2. Advance of cold front from formation until dissipation. Day and hour of frontal positions are written on the left end of the front. The trajectory of the associated extratropical cyclone is shown as a dotted line; circled dots indicate position every 12h, and the central pressure is underlined. The trajectory of the polar anticyclone, with central pressure similarly indicated, is shown by the dashed line. Taken from Fortune and Kousky (1983).

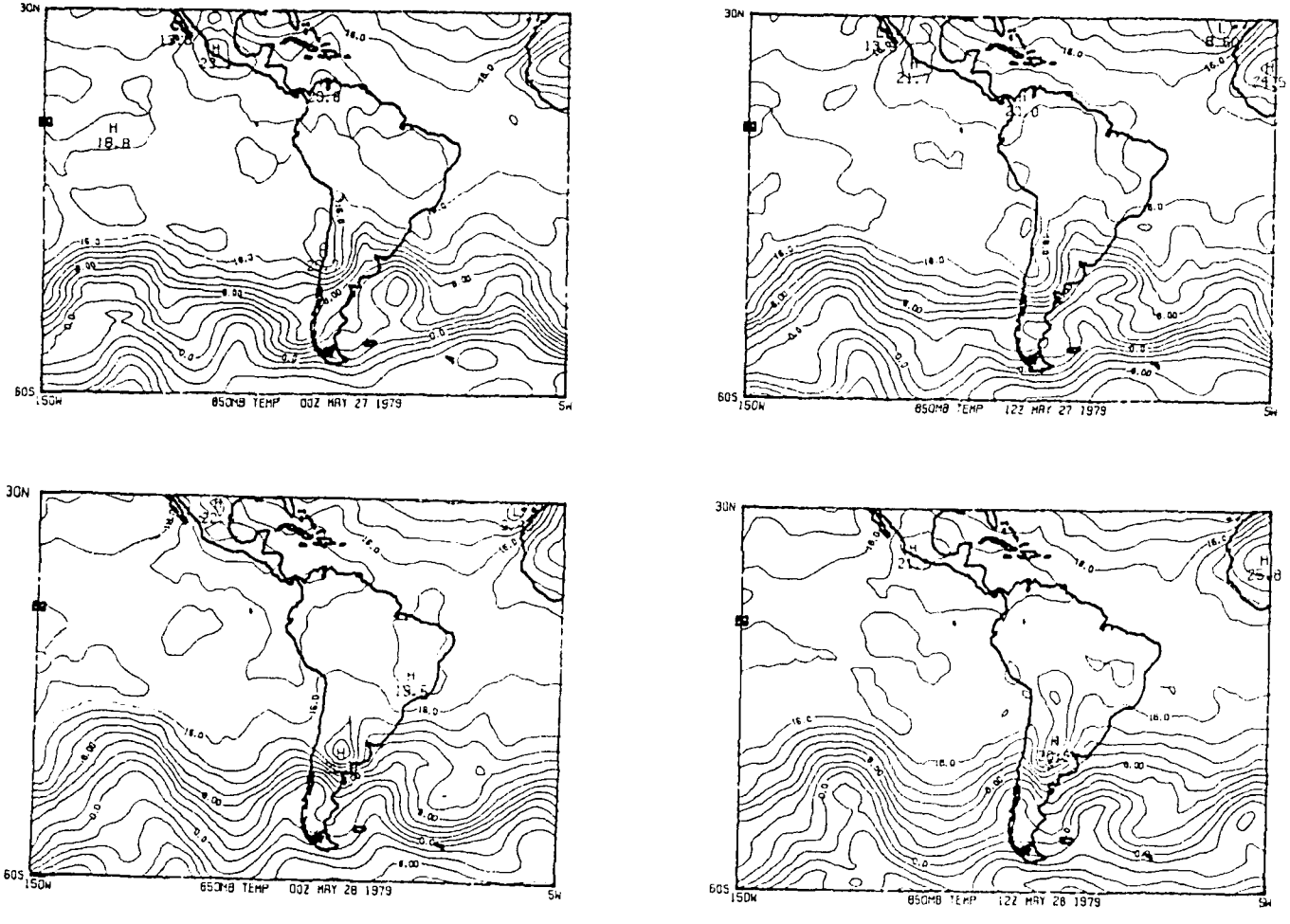


Figure 3. 850 mb isotherms with intervals of 2°C for 27 May and 28 May.

over the southern regions of South America associated with a longwave trough in the region. At 0000 UTC 28 May another cold trough develops off the southwest coast of South America. This trough may have been partially induced by the cold water temperatures due to upwelling off the Chile coast, but most likely it was due to strong advection of cold air from the south (see 850 mb wind vectors, Chapt. V.2). On 28 and 29 May both cold troughs intensify. The cold trough to the west appears to move over the Andes, and by 0000 UTC 30 May the two cold troughs merged off the east coast of Argentina. The 850 mb wind field in the region (see Chapt. V.2) indicates strong southerly winds at approximately 15-20 m/s. Thus the cold advection is extremely intense (approximately 0.5°C per hour on 30 May) from northern Argentina to Southern Brazil. The freeze at the surface occurred in southern Brazil on the mornings of 31 May and 1 June, at 850 mb the 0°C isotherm is located in northern Argentina. On 31 May (Fig. 4) the relatively the cold trough air extends into central Brazil, and from the strong temperature gradient, it appears the front was strongest at this time. By 00Z on 1 June the 0°C the winds turned to more southwesterly direction, the temperature advection weakened and the 0°C isotherm regressed far to the south (Fig. 5).

## IV.2 The Tropical Cyclones

The tropical cyclone season in the eastern North Pacific normally begins in late May or early June. The year of 1979 was a typical year; a tropical disturbance was identified at 1800 UTC 29 May and was classified as the first tropical depression of the season at 1800 UTC 31 May. Just prior to this another disturbance was sighted

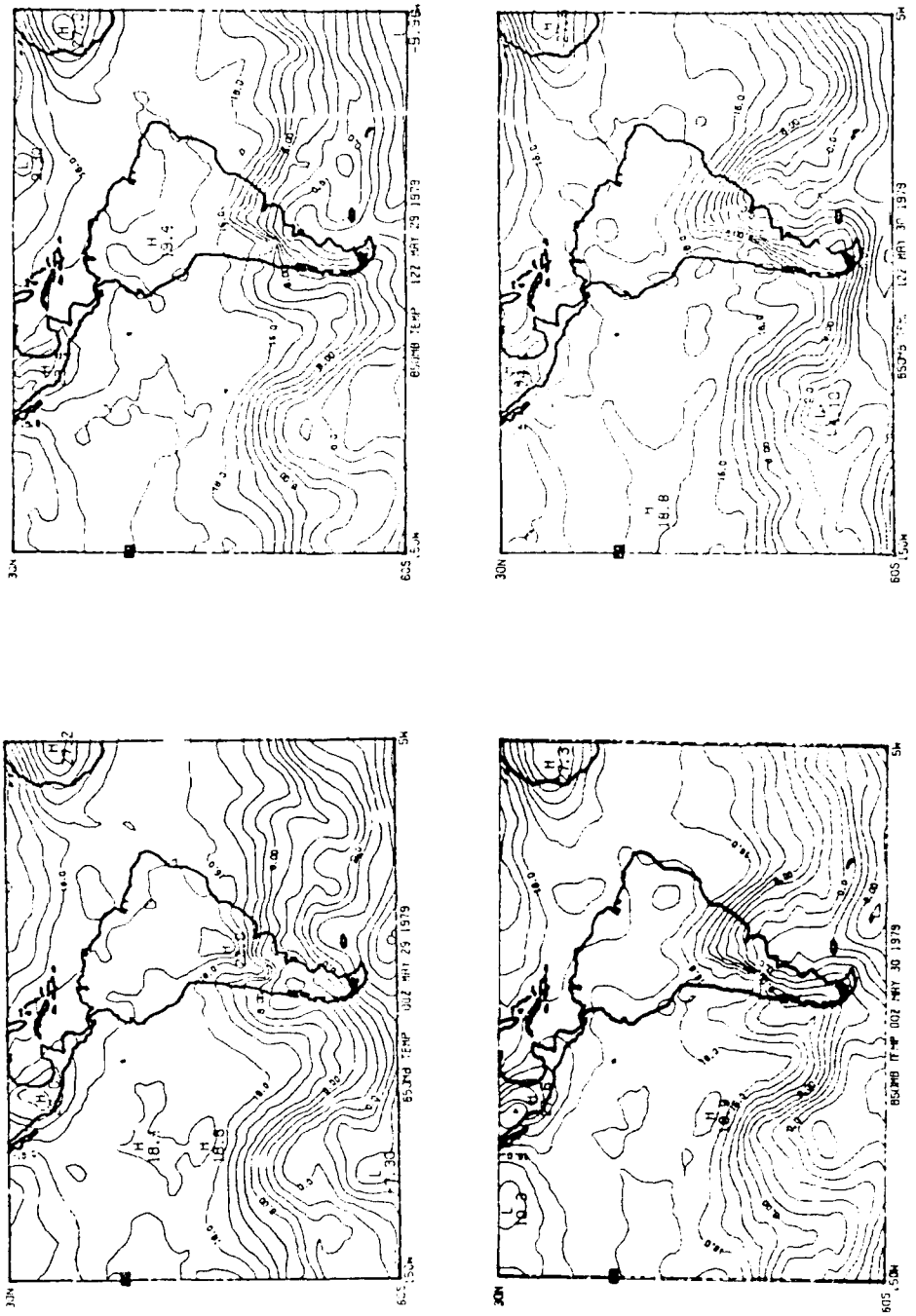

Figure 4. 850 mb isotherms with intervals of 2°C for 29 May and 30 May.

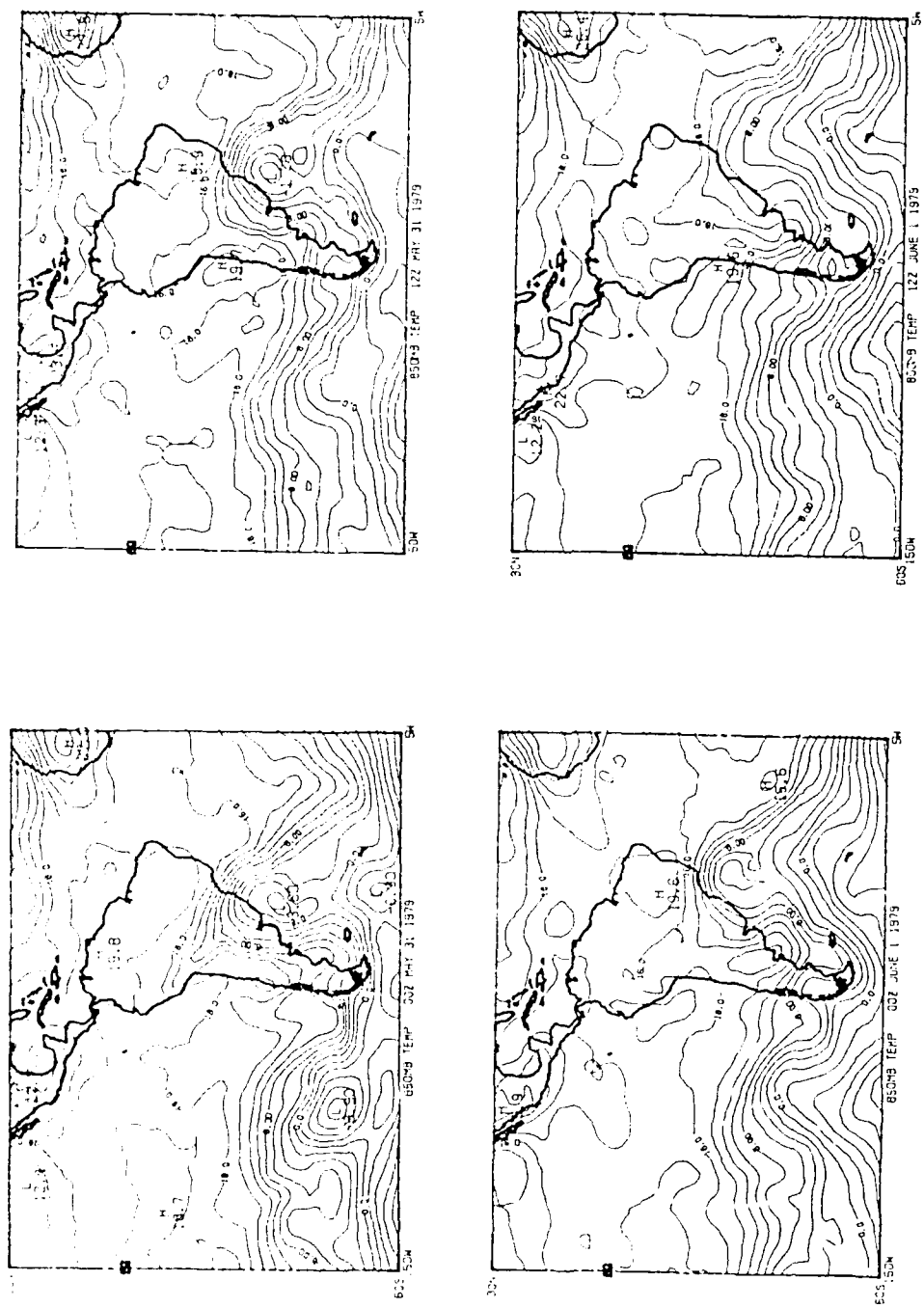

Figure 5. 850 mb isotherms with intervals of 2° for 31 May and 1 June.

at 0000 UTC 31 May and upgraded to a tropical depression also at 1800 UTC 31 May. It is very uncommon for two depressions to form on the same day this early in the season. In fact it is the only time in recorded history that two cyclones have developed simultaneously in May.

The movement of the tropical cyclones is shown in Fig. 6. The first cyclone, Tropical Depression One, was very short lived. The disturbance was first sighted at 1800 UTC on 29 May 300 nm south of Manzanillo, Mexico and was upgraded to a tropical depression at 1800 UTC 31 May near 13.5°N, 107.5°W. It moved northwesterly at 7 kts, and rapidly weakened. The last advisory was issued at 0000 UTC 1 June when it was located at 14.0°N, 108.0°W (Gunther, 1980).

The second cyclone, Hurricane Andres, began as a tropical disturbance at 0000 UTC 31 May 300 n mi south of the Gulf of Tehuantepec, and was upgraded to a depression at 1800 UTC 31 May. It moved westerly and then northwesterly until on 4 June it moved onshore 215 nm west northwest of Acapulco. Between 31 May and 4 June the wind was reported to be between 25 and 80 kts, with heavy, continuous rain and a minimum pressure of 995.0 mb (Gunther, 1980).

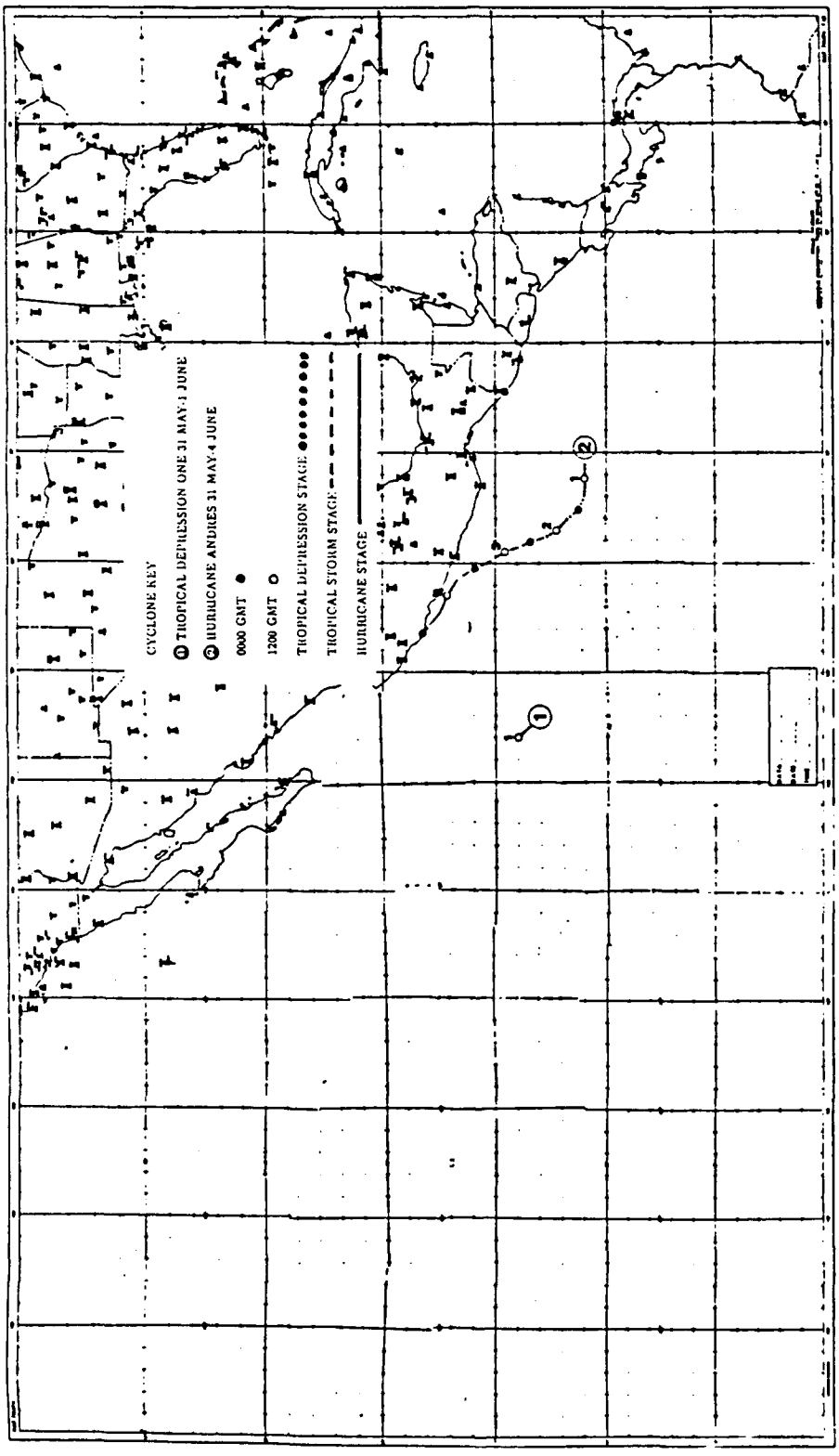


Figure 6. Tropical depression 1 and Hurricane Andres tracks. Taken from Gunther (1980).

# CHAPTER V

# SMALL SCALE DIAGNOSTICS

It is not obvious from examining the Southern Hemisphere cold front and tropical cyclone formation in the eastern North Pacific separately that there was a link between them. To determine if there was a cross-equatorial interaction between the systems, a diagnostic study must be conducted. If an interaction is discovered, then it must be determined if this interaction was such that it was influential in the development of the tropical cyclones.

## V.1 Temporal Variation of OLR

OLR composites were developed for 27 May to 1 June 1979. The average was taken of the 0000 UTC and the 1200 UTC OLR fields for each day to remove the diurnal cycle. OLR data cannot be used to determine circulation features and vertical structures; however, used in conjunction with other data sources, OLR provides an additional perspective as well as verification of the features seen in other data.

The OLR field depicts the cloud pattern associated with the Southern Hemisphere frontal movement. The composites indicate on 27 May (Fig. 7) two regions of low OLR values associated with the two Southern Hemisphere lows: one off the southern tip of South America and the other off the southeast coast of South America. To the north, the equatorial trough is active in the eastern North Pacific throughout the period, and the Amazon basin is also strongly convective. In association with the superposition of the waves and the amplification of the Southern Hemisphere

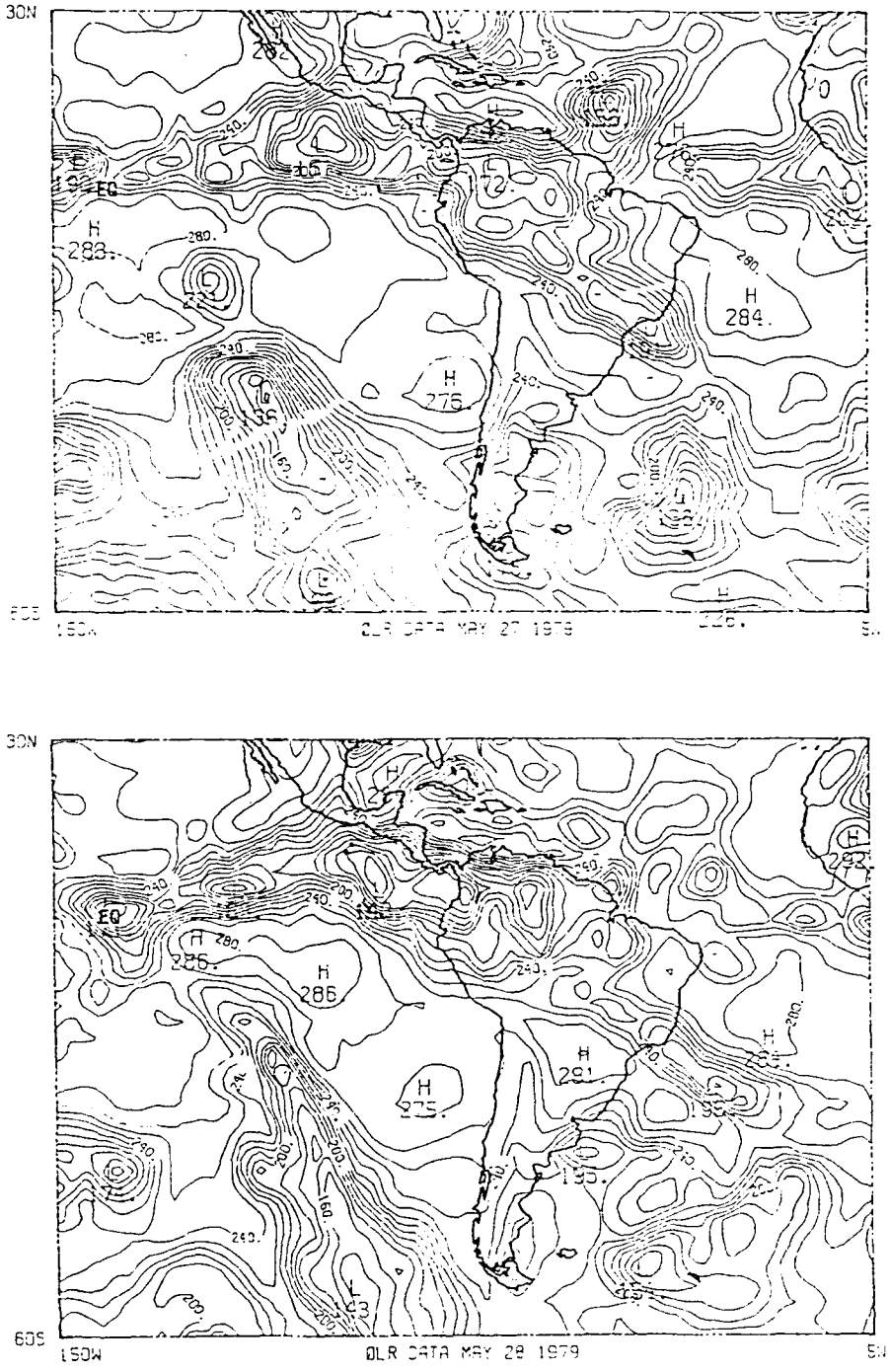


Figure 7. Outgoing longwave radiation for 27 and 28 May. Units are W/m$^2$ and the contour interval is 10 W/m$^2$.

trough, low OLR values of less than 200 $W/m^2$ are present off the southeastern coast of Brazil on 29 and 30 May (Fig. 8). On 30 May the cloud field associated with the frontal band is unmistakable. Low values of OLR extend from the low pressure center northeastward until it merges with the clouds associated with the equatorial trough of the Northern Hemisphere. The intense high pressure behind the front, associated with the freeze in Brazil, also shows up as relatively high values of OLR behind the frontal band. The band of low OLR values begins to break up on 31 May and 1 June (Fig. 9) indicating the trough is weakening and moving to the east. However, even though there is not a distinct band of low OLR values, the values remain relatively low over the region.

Throughout the period the OLR indicates the equatorial trough was unusually active. Typically tropical cyclones in this region of the world develop in the equatorial trough. The tropical cyclones under investigation were no exception. The OLR indicates that values were very low prior to tropical cyclone genesis, with minimum values as low as 109 $W/m^2$ on May 29. Australian and Chinese forecasters believe that what occurs in the equatorial trough is determined in some way by the events in both the Northern and Southern Hemispheres (Love, 1982). Looking at the OLR field on 30 May, it is difficult to discount this possibility. Low OLR values extend all the way from the Southern Hemisphere front northwestward into the equatorial trough, suggesting an interaction between the Southern Hemisphere front and the equatorial trough. Whether this interaction was such that it was influential in the development of these tropical cyclones will be determined by further diagnostic studies.

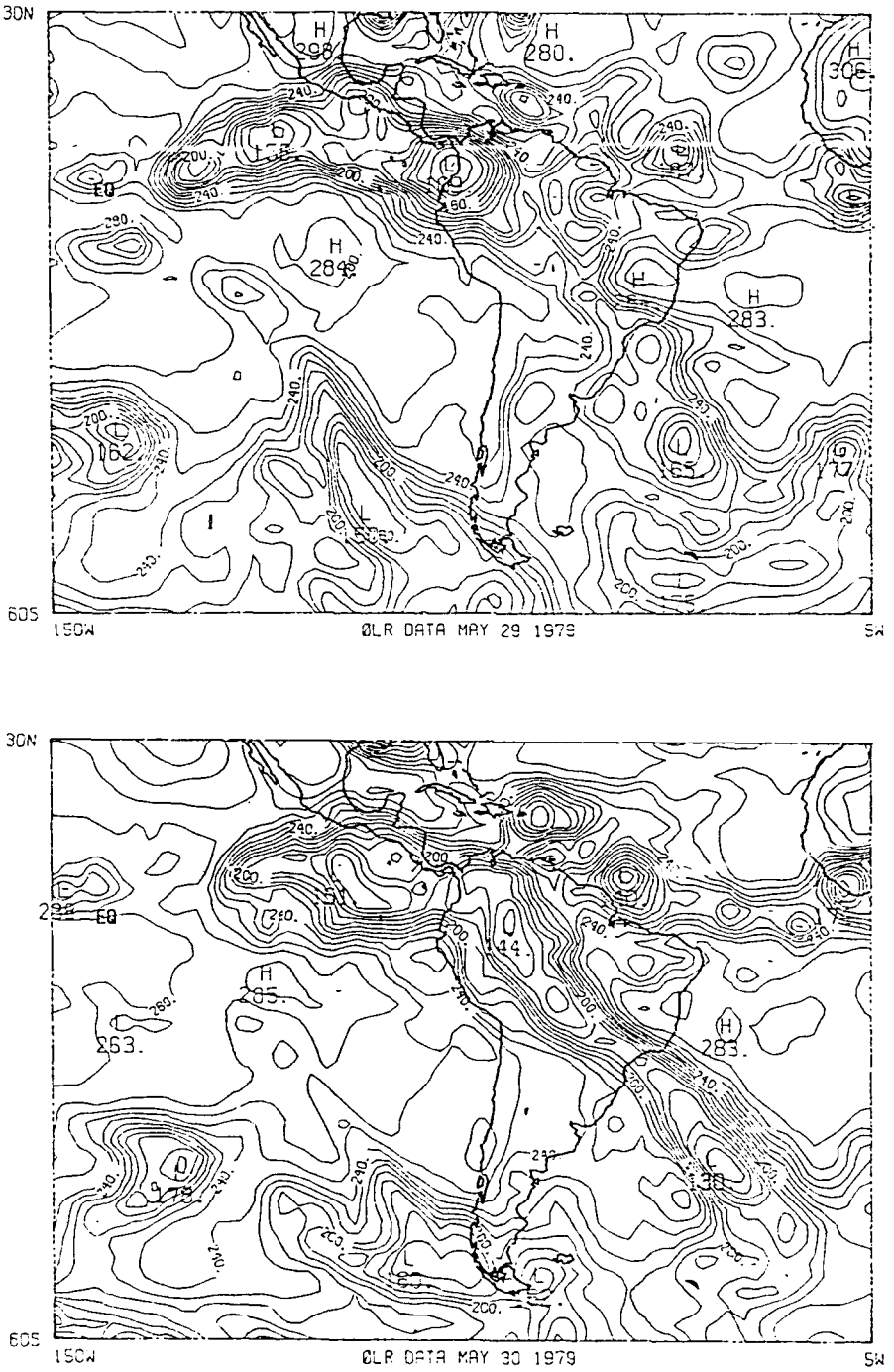


Figure 8. Outgoing longwave radiation for 29 and 30 May. Units are $W/m^2$ and the contour interval is 10 $W/m^2$.

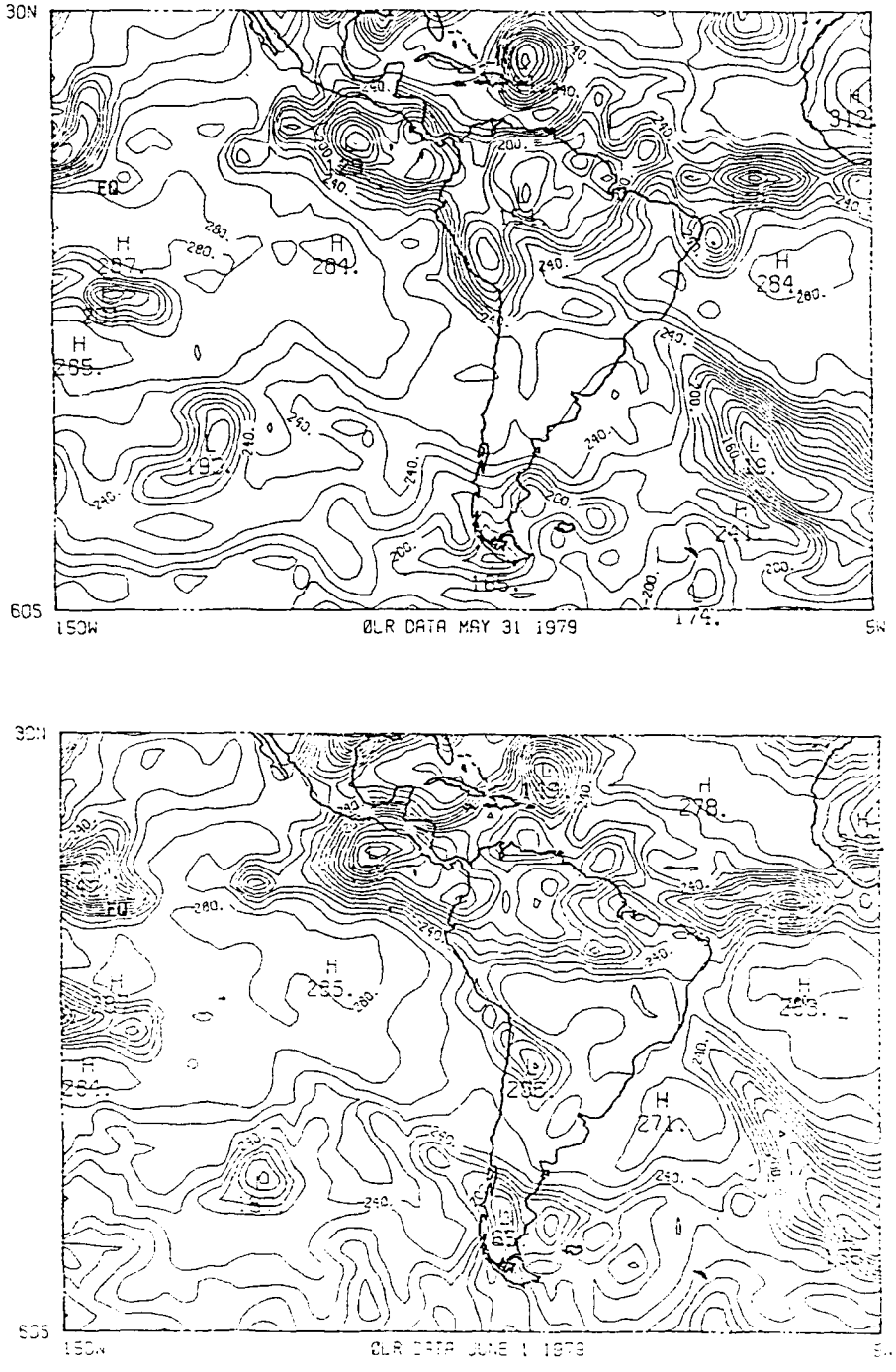


Figure 9. Outgoing longwave radiation for 31 May and 1 June. Units are $W/m^2$ and the contour interval is 10 $W/m^2$.

## V.2 Low-Level Diagnostics

Tropical cyclone development is strongly dependent on the pre-existence of a favorable large scale environment (Gray, 1968; Gray, 1975; McBride and Zehr, 1981). Climatology is such in the eastern North Pacific that Gray's thermodynamic tropical cyclone genesis criteria (warm sea surface temperatures, high mid level humidity, strong vertical equivalent potential temperature gradient, see Chapt. II) are nearly always present in late May and early June. Gray's wind shear criterion is also satisfied in this area of the world: the equatorial trough region typically has a very small vertical wind shear. However, the vorticity criterion is not always satisfied. Vorticity changes very quickly in the atmosphere, on the order of days. McBride (1981) studied the effect of vorticity on tropical cyclone genesis. He found the difference between developing and non-developing cloud clusters in the tropics was that developing cloud clusters were located in regions of high values of low-level vorticity while non-developing cloud clusters were associated with low values of relative vorticity. Therefore, it is appears that high positive relative vorticity associated with large-scale cyclonic flow is a crucial feature for tropical cyclone genesis.

### V.2.1 Low-Level Vorticity increases in the Region of Tropical Cyclone Genesis

A vorticity study at 850 and 500 mb was conducted in the region of tropical cyclone formation for the period of 0000 UTC 27 May to 1200 UTC 1 June. The vorticity at each grid point was calculated using the vorticity definition:

$$\zeta = \frac{\partial v}{\partial x} - \frac{\partial (u cos\theta)}{cos\theta \partial y}$$

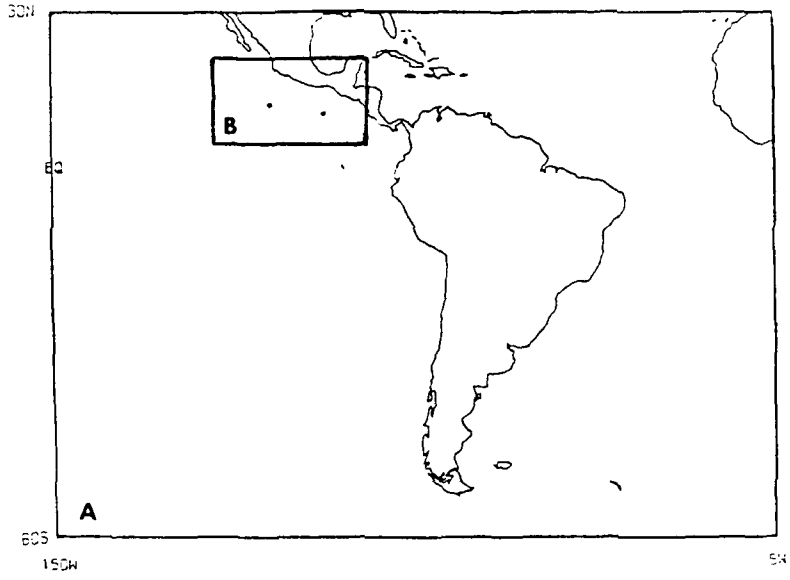


Figure 10. Vorticity calculation region. Region B within the domain (A) was used to compute the average vorticity. The locations of tropical cyclone genesis are shown as dots.

Then the average was taken over region B (Fig. 10). Since we are interested in the large-scale vorticity field, region B was chosen to encompass not only the area directly over the tropical cyclone genesis, but also to include a region of approximately 200–300 km surrounding the region of genesis and over a region where the climatological equatorial trough is located. A time series of the average vorticity for the boxed region for the period 0000 UTC 27 May to 1200 UTC 1 June (Fig. 11) reveals that at 850 mb there is a gradual increase in the vorticity in the boxed region. It begins as slightly negative but gradually increases, becoming positive at

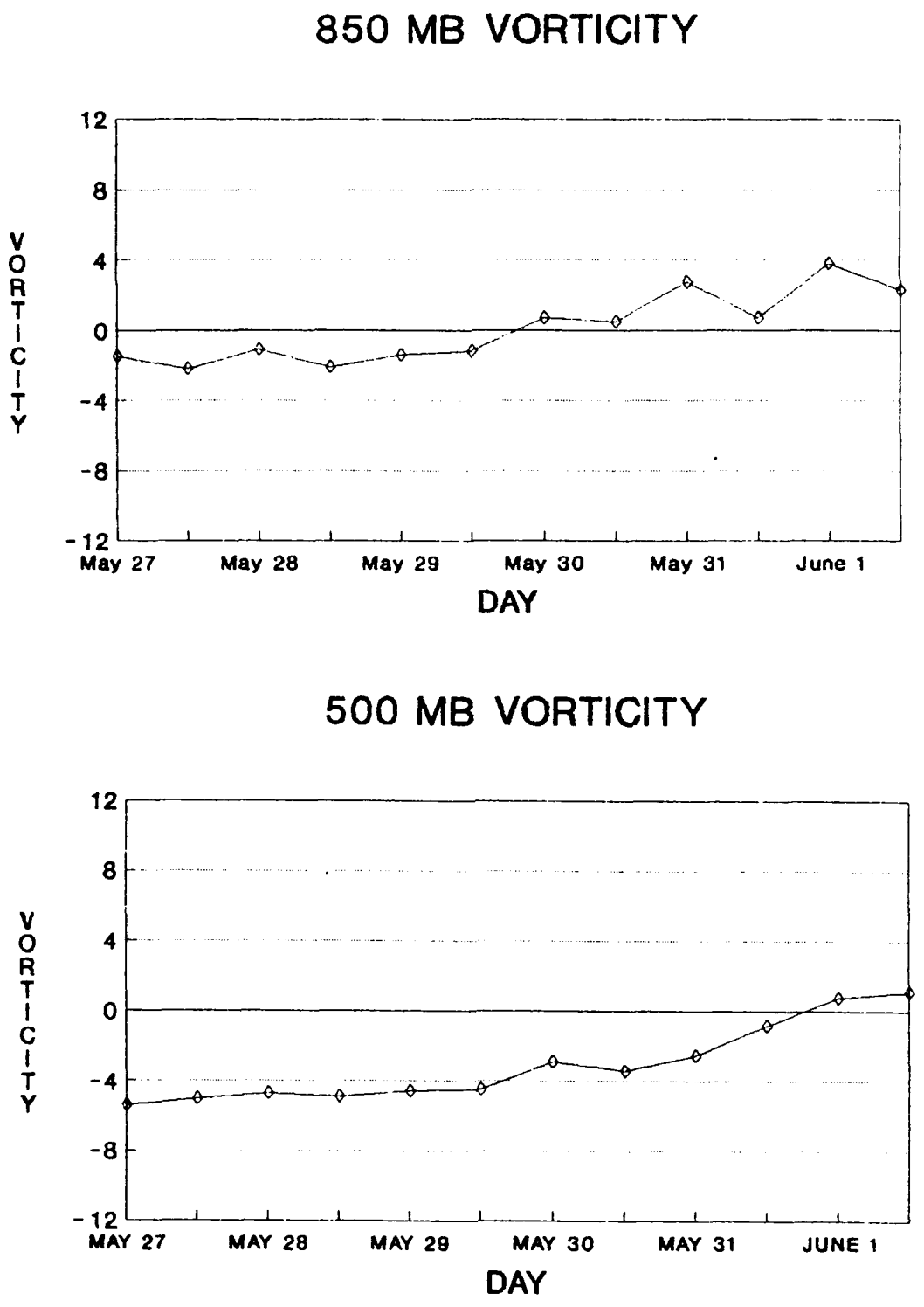


Figure 11. Vorticity. Time series of average vorticity over region B at 850 mb (top) and 500 mb (bottom). Vorticity units are 1 x $10^{-5}$ $s^{-1}$.

approximately 1800 UTC 30 May. Although somewhat noisy, it continues to increase through the time of tropical cyclone genesis at 1800 UTC on 31 May (Fig. 5). The 500 mb average vorticity over region B shows a similar trend: at 0000 UTC 27 May the vorticity is negative, but gradually increases and becomes positive at approximately 1800 UTC 31 May, the time of tropical cyclone genesis.

These results are consistent with earlier studies that low-level vorticity does increase in the vicinity of tropical cyclone genesis; however, it is not clear if this increase in vorticity was in any way tied to events in the Southern Hemisphere.

V.2.2 850 mb Winds and Streamlines

The wind field is very useful for identifying circulation features in the tropics. Typically in the mid-latitudes, circulation features are identified through pressure or geopotential height. However, in the tropics where the atmosphere is generally barotropic, analyses of these elements are of little use. In this study, if any inter-hemispheric interaction between the cold surge and tropical cyclone genesis occurs, it is likely to occur in the tropics; therefore, wind analysis was used rather than geopotential height analysis to track the synoptic features. The total wind field at 850 mb was produced from x and y wind components for the period 27 May–1 June at 0000 UTC and 1200 UTC. To further clarify the total wind field, hand drawn streamline analyses were superimposed over the computer generated wind vectors.

At 0000 UTC 27 May (Fig. 12) the streamlines reveal that the two mid-latitude cyclones ($C_1, C_2$) are located on either side of the southern cape of South America. The subtropical ridge is displaced northward into north central Brazil, and the associated counter-clockwise flow extends across the equator into the Northern Hemisphere in the vicinity of Central America. As the counter-clockwise flow crosses the equator, the anticyclonic circulation associated with it becomes cyclonic in the Northern Hemisphere.

At 0000 UTC 28 May (Fig. 13) a South Atlantic anticyclone ($A_1$) moves northward and intensifies. Cyclone $C_1$ remains nearly stationary. As Cyclone $C_2$ approaches cyclone $C_1$, a trough develops which extends northward into northern Chile. $C_2$ continues to advance and at 0000 UTC 28 May catches up with $C_1$, superimposing to the northwest of the Falkland Islands sometime between 0000 UTC and 1200 UTC 28 May. The trough develops to the northwest across the Andes, and extends off the coast of northern Chile. Meanwhile, just west of Ecuador, vortex $E_1$ forms. This vortex develops in the counter-clockwise flow associated with the extension of the northern South American subtropical ridge into the Northern Hemisphere.

At 0000 UTC 29 May (Fig. 14) the Southern Hemisphere trough further amplifies west of the Andes until it extends nearly to the equator, breaking through the subtropical ridge. As the trough develops equatorward eddy $E_1$ is severed from the ridge axis just west of Ecuador. At 1200 UTC 29 May $E_1$ continues to intensify and expands further into the Northern Hemisphere. To the south, a small cyclone

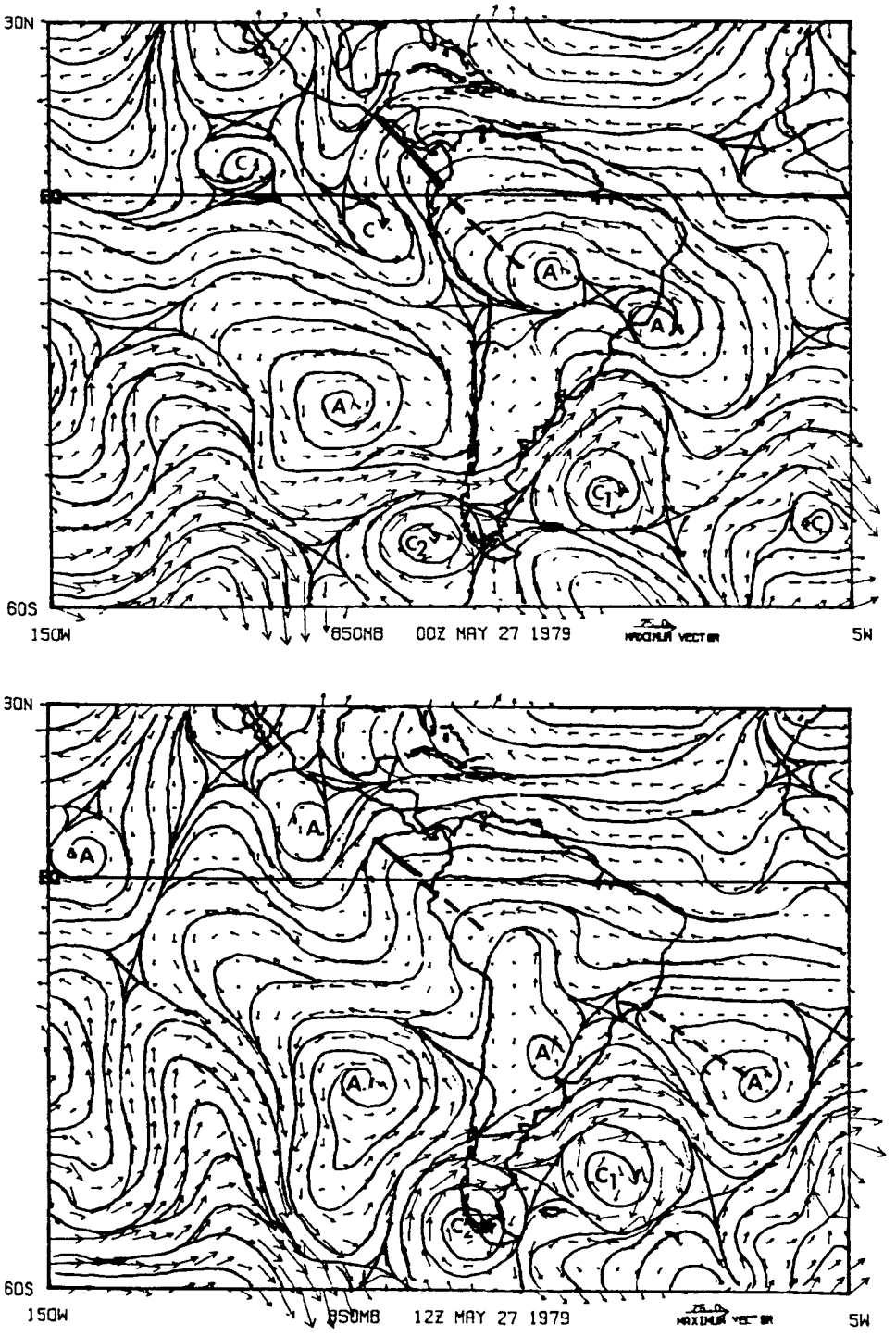


Figure 12. 850 mb winds for 27 May. Wind vectors are shown as arrows (reference vector is 25 m/s) and streamlines are shown as solid lines at 0000 UTC (top) and 1200 UTC (bottom). Solid heavy lines represent troughs and broken heavy lines represent ridges.

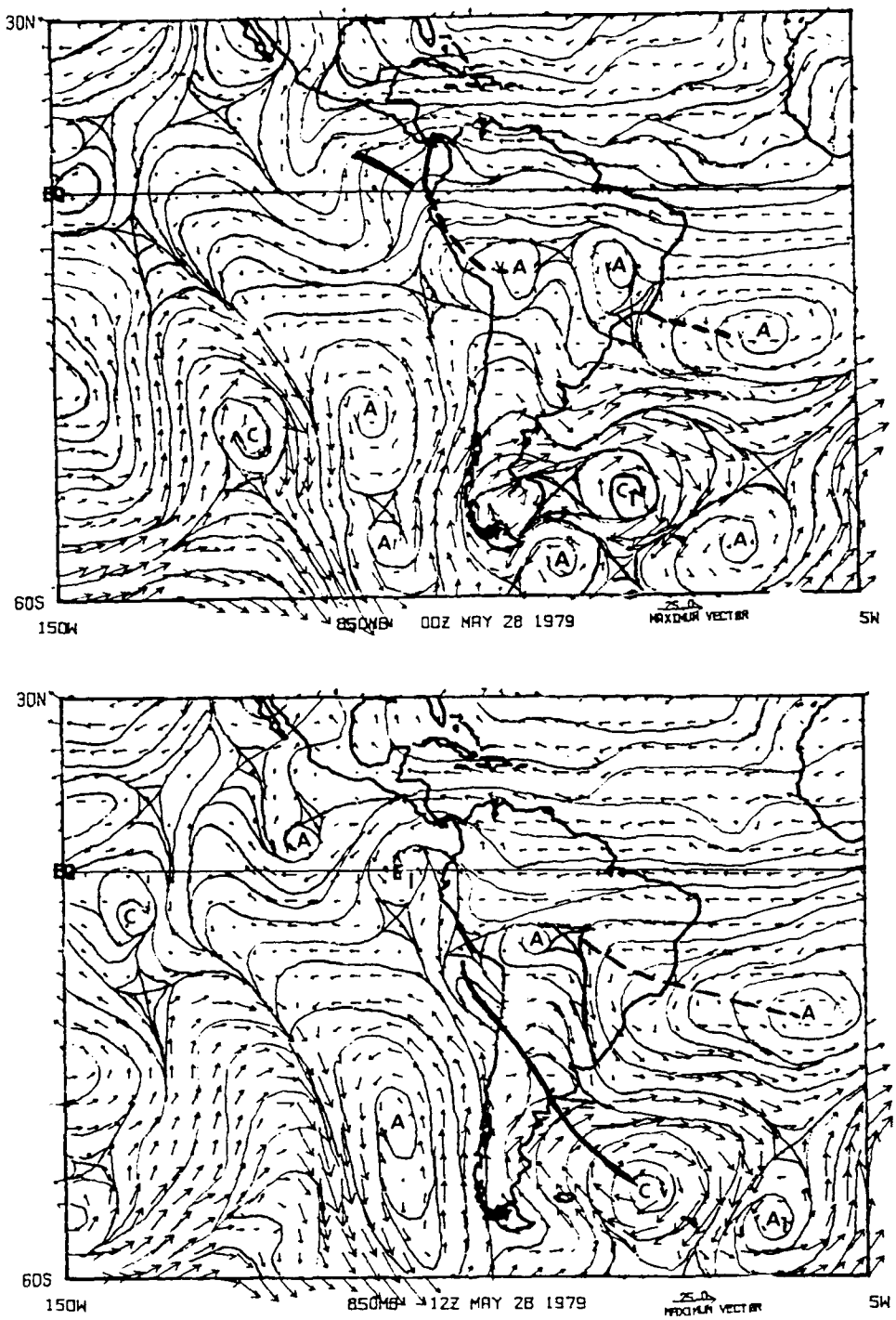


Figure 13. 850 mb winds for 28 May. Wind vectors are shown as arrows (reference vector is 25 m/s) and streamlines are shown as solid lines at 0000 UTC (top) and 1200 UTC (bottom). Solid heavy lines represent troughs and broken heavy lines represent ridges.

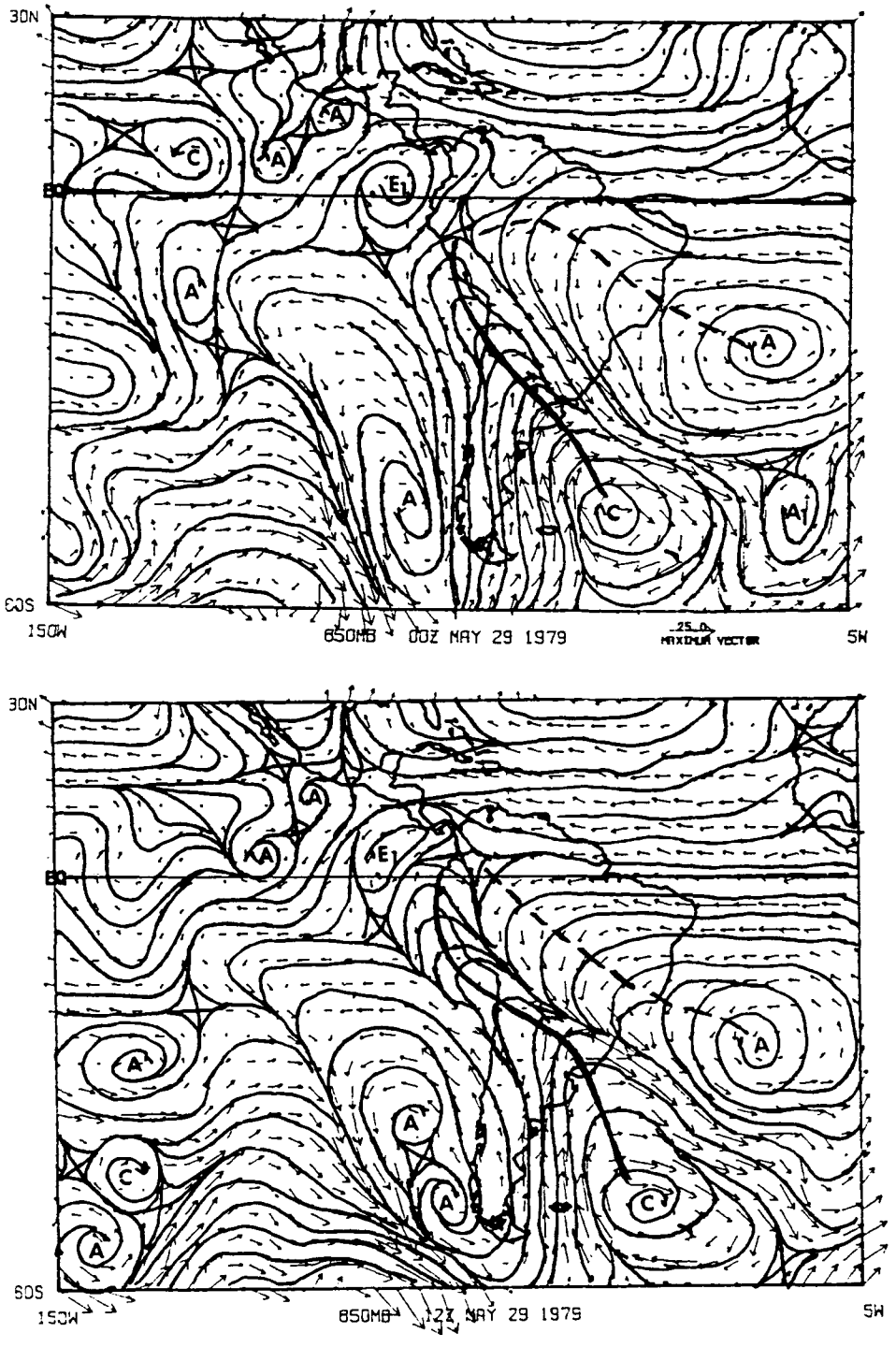


Figure 14. 850 mb winds for 29 May. Wind vectors are shown as arrows (reference vector is 25 m/s) and streamlines are shown as solid lines at 0000 UTC (top) and 1200 UTC (bottom). Solid heavy lines represent troughs and broken heavy lines represent ridges.

($C_3$) forms in the northern regions of the trough off the coast of Peru at 0000 UTC 30 May. At 0000 UTC 30 May (Fig. 15) the Southern Hemisphere trough moves eastward, and $C_3$ is left behind on the west side of the Andes. Eddy $E_1$ moves northward into the Northern Hemisphere, develops into an elongated cyclone ($C_4$), merging with the equatorial trough (the location of the equatorial trough can be seen in the OLR composites, see section V.1). In the previous section it was shown that there was a gradual increase in the vorticity in the days prior to tropical cyclone genesis; the migration of this eddy northward appears to have contributed to the vorticity increase. To the east we see westerlies begin to develop just north of the equator from approximately 90°W to 115°W.

At 1200 UTC 30 May and 0000 UTC 31 May the westerlies between 90°W and 110°W strengthen just north of the equator. These westerlies combine with weaker westerlies to the north (at approximately 10°N) to create cyclonic shear and increase the large-scale vorticity in the region of tropical cyclone genesis (Fig. 16). The westerlies rapidly weaken following tropical cyclone formation at approximately 1800 UTC 1 June (Fig. 17) .

To summarize, at 850 mb the Southern Hemisphere subtropical ridge was displaced northward. The southern hemisphere wave strongly amplified and severed a small equatorial eddy from the Southern Hemisphere subtropical ridge. The eddy moved northward merging with equatorial trough, increasing the low-level vorticity in the region of tropical cyclone genesis. Vorticity produced by shear due to relatively strong westerlies south of the region of tropical cyclone genesis appears to have also

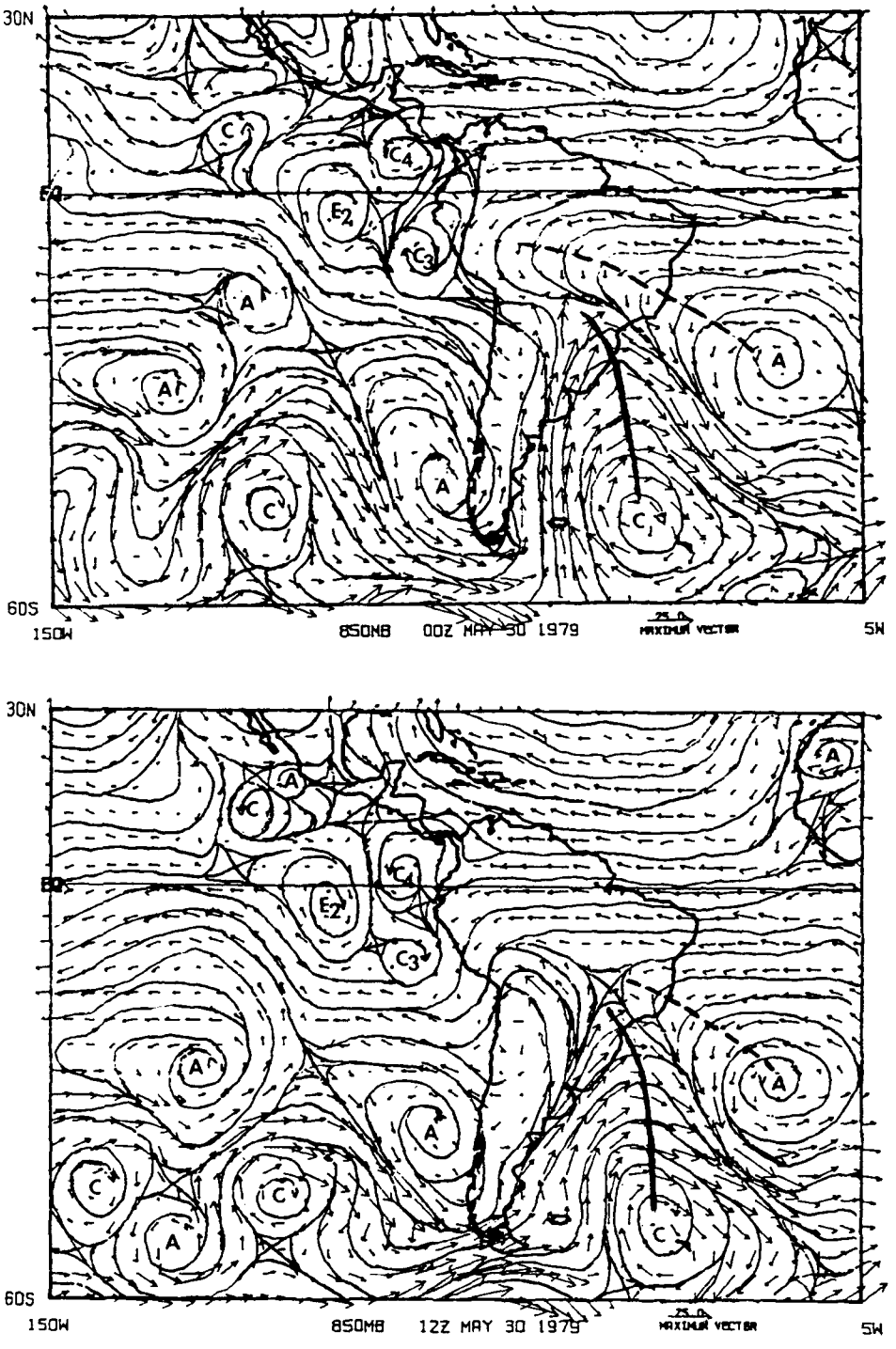


Figure 15. 850 mb winds for 30 May. Wind vectors are shown as arrows (reference vector is 25 m/s) and streamlines are shown as solid lines at 0000 UTC (top) and 1200 UTC (bottom). Solid heavy lines represent troughs and broken heavy lines represent ridges.

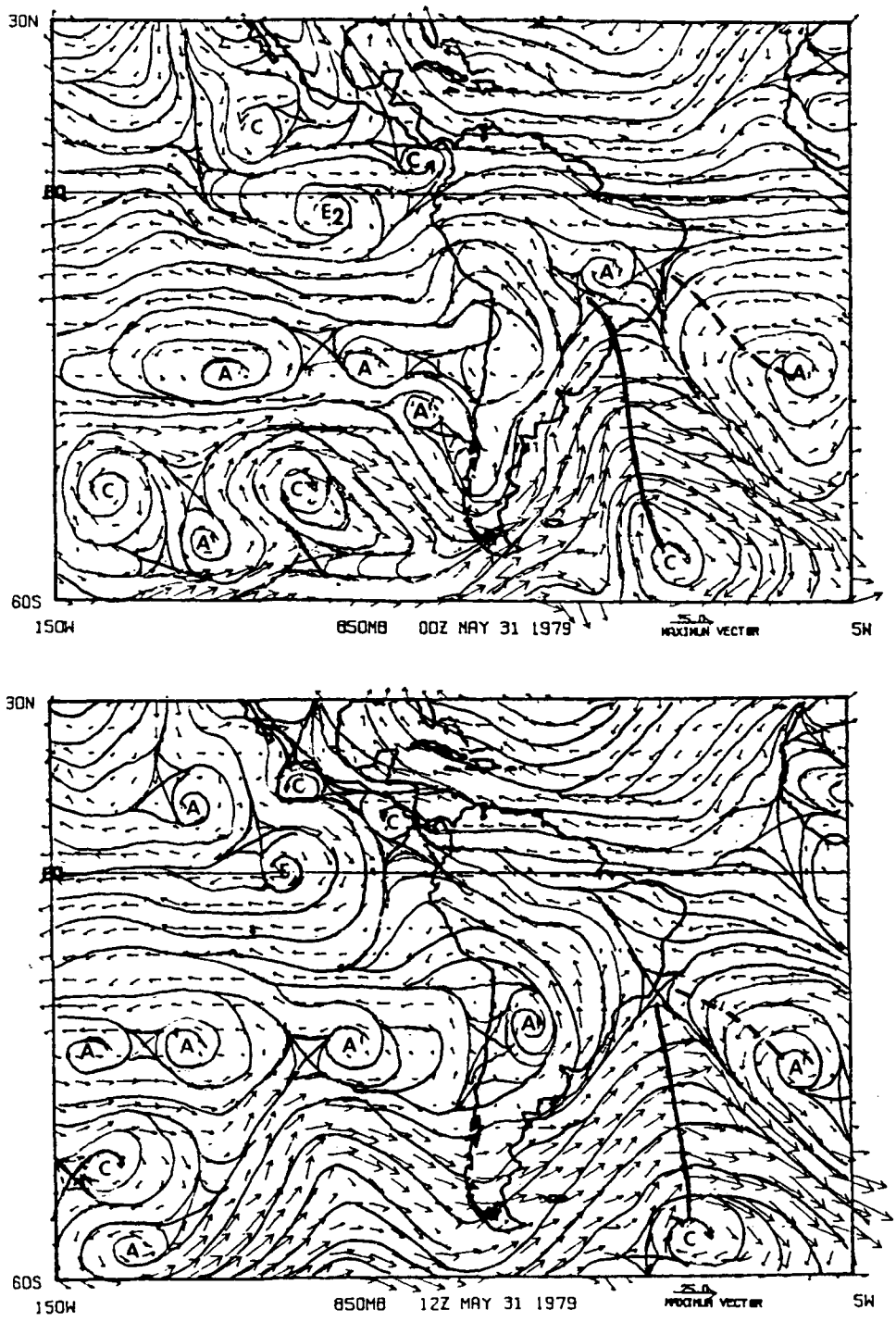


Figure 16. 850 mb winds for 31 May. Wind vectors are shown as arrows (reference vector is 25 m/s) and streamlines are shown as solid lines at 0000 UTC (top) and 1200 UTC (bottom). Solid heavy lines represent troughs and broken heavy lines represent ridges.

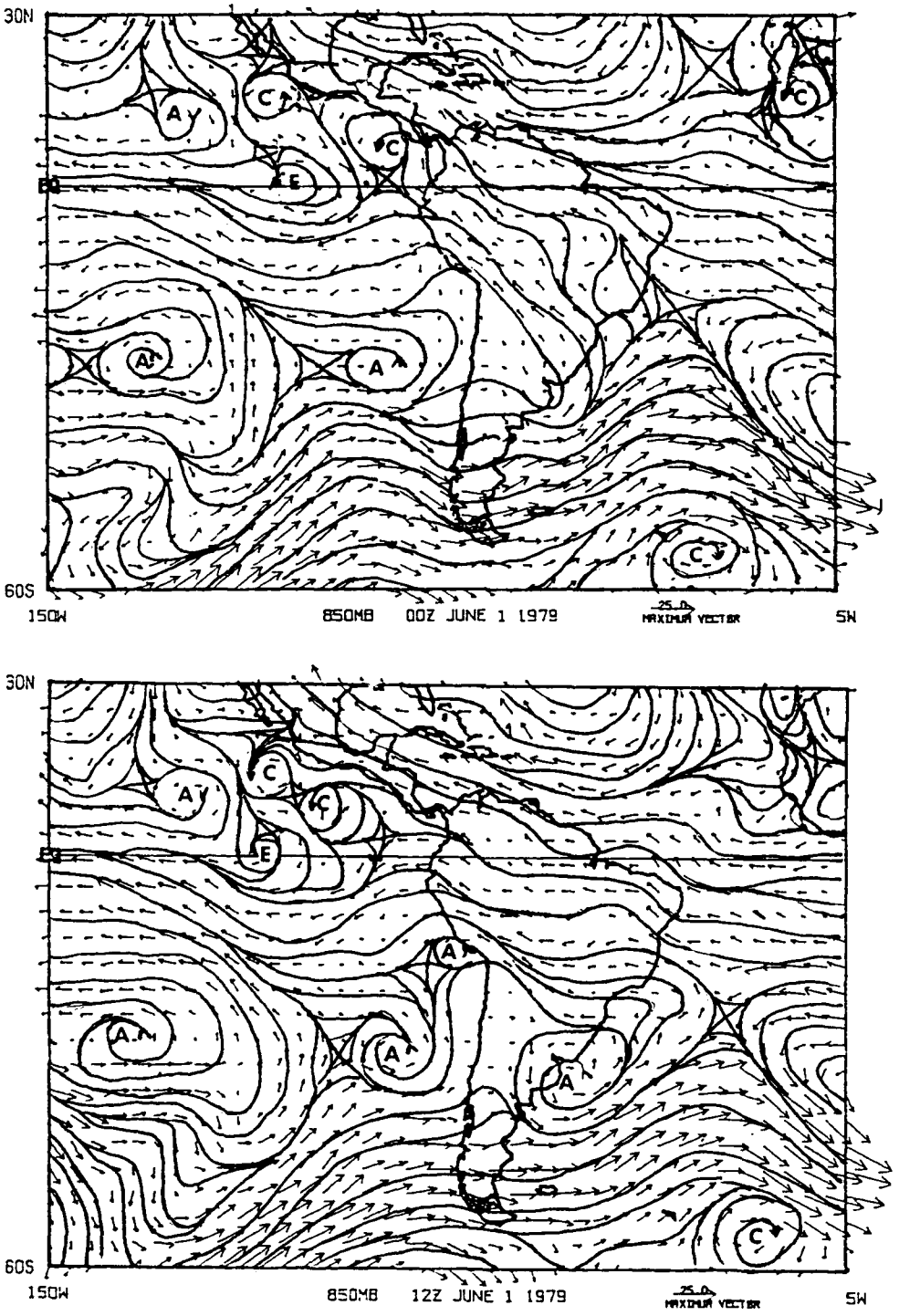


Figure 17. 850 mb winds for 1 June. Wind vectors are shown as arrows (reference vector is 25 m/s) and streamlines are shown as solid lines at 0000 UTC (top) and 1200 UTC (bottom). Solid heavy lines represent troughs and broken heavy lines represent ridges.

increased the large scale low-level vorticity, and thus appears to have been influential in the development of the two tropical cyclones.

V.2.3 Love's Theory

Love (1982) conducted two case studies on the effect of cold surges on tropical cyclone development in the opposing hemisphere. Both events occurred in the West Pacific: the first genesis event occurred in the Southern Hemisphere at approximately 120°E and the second in the northern hemisphere at approximately 150°E. Love found that in both cases a winter hemisphere equatorward surge of cold air led to rising pressures in the subtropical ridge of the winter hemisphere and subsequent equatorial surface pressure increases of approximately 2 mb. He also found enhanced westerly flow in the equatorial regions from the surface to 500 mb and theorized that this was a result of down gradient or an isallobaric wind due to the east-west pressure gradient produced by the pressure rise. Increased low-level westerly flow on the equator is associated with increase positive vorticity due primarily to shear vorticity. In an effort to determine if Love's theory is applicable to the case study presented in this thesis, the 850 mb geopotential height field was examined to determine if an equatorial pressure rise associated with the South American cold surge could be identified. It is clear from the streamline analysis in the previous section that strong westerlies were present prior to tropical cyclone genesis. The 0000 UTC and 1200 UTC geopotential heights were averaged to remove any diurnal effects and then plotted for 15°N to 15°S

for 29 May (2 days prior to tropical cyclone genesis) and 31 May (the day of tropical cyclone genesis). The difference between these two fields was also plotted (Fig. 18) .

On 29 May (Fig. 18a) low geopotential heights associated with the amplification of South American trough extend into Colombia. To the west-southwest, the ridge axis of the Southern Hemisphere anticyclone is depicted by the high geopotential heights extending to the northwest from approximately 85°W, 30°S to 110°W, 5°S. In the Northern Hemisphere a trough extends south over Central Mexico with geopotential heights as low as about 1480 gpm. A large high dominates the region to the west, from approximately 130°W to 150°W and 15°N to 30°N. In the equatorial regions to the south lower geopotential heights dominate from approximately 120° to 150°W.

By 31 May (Fig. 18b) the Southern Hemisphere subtropical ridge has greatly expanded. An anticyclone has developed over South America, replacing the trough as indicated by the high geopotential heights in the region. The subtropical ridge now dominates the entire Eastern Pacific from 10°S to 30°S. The Southern Hemisphere subtropical ridge appears to have built to the Northwest, but there is only weak penetration into the equatorial regions at approximately 120°W to 140°W. In the Northern Hemisphere, the trough over Mexico has strengthened somewhat as indicated by the decrease in geopotential heights from 1480 gpm to 1465 gpm. This decrease extends southward off the west coast of Central America, indicating a deepening of the equatorial trough. Geopotential height increase reveals that the Northern Hemisphere anticyclone to the west has also intensified.

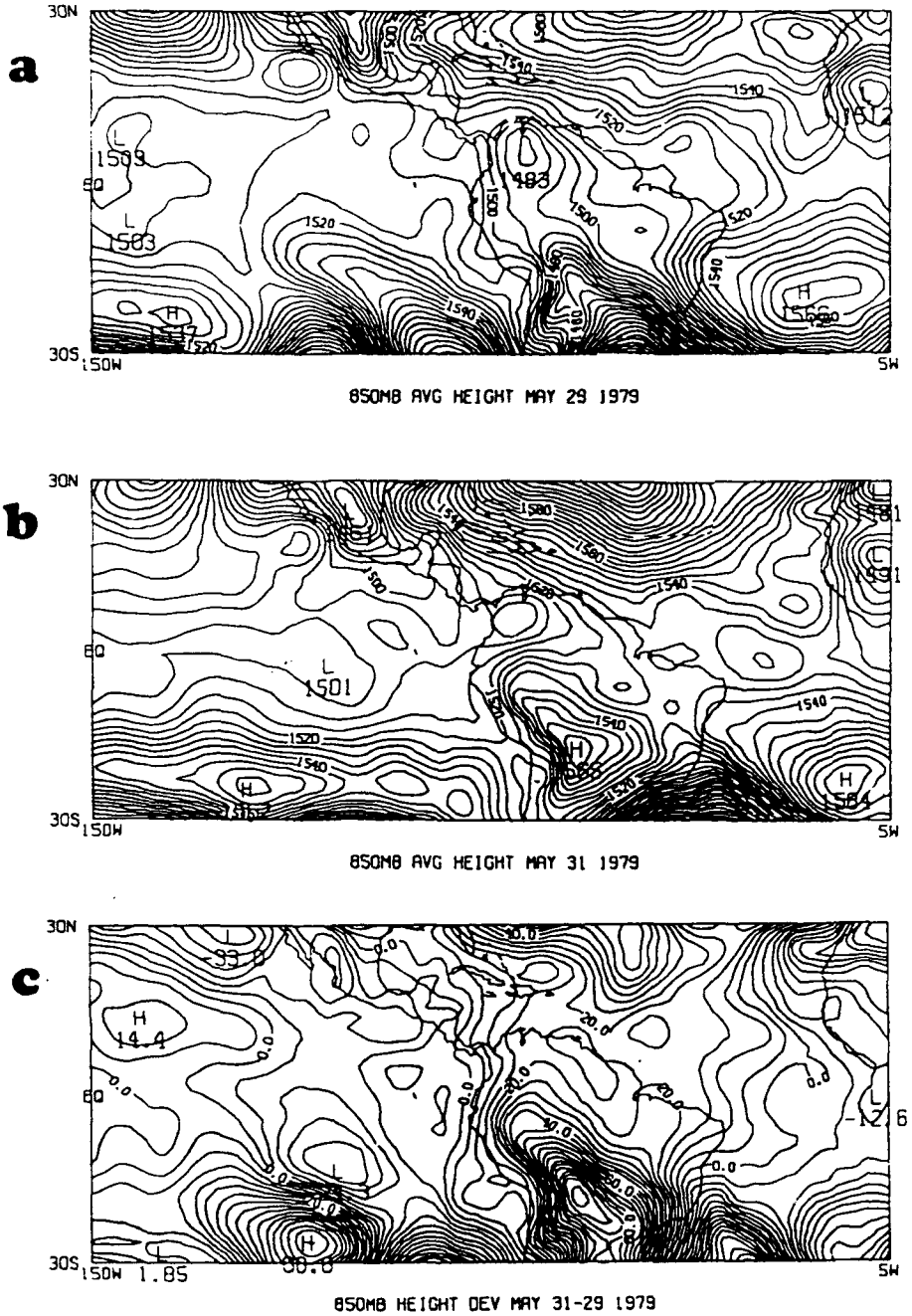


Figure 18. 850 mb geopotential height from 15°N to 15°S. Averaged 0000 UTC and 1200 UTC geopotential height for 29 May (a) and 31 May (b), 31 May minus 29 May geopotential height (c). Contour intervals are 5 gpm.

The largest changes (Fig. 18c) are associated with the building of the Southern Hemisphere subtropical ridge over the eastern subtropical Pacific. In the equatorial regions, where we would expect very small changes in the geopotential height field, there is in fact a rather dramatic change between the two days. In the western portion of the domain, from approximately 120°W to 150°W, the geopotential height has increased as a result of both the Southern and Northern Hemisphere subtropical anticyclones building equatorward. However, the strongest increase is associated with the Northern Hemisphere anticyclone, not the Southern Hemisphere anticyclone as Love's studies had indicated. In the equatorial region to the east, from approximately 80°W to 120°W, the geopotential height has fallen in association with the deepening of the equatorial trough in the Northern Hemisphere and the building of the subtropical ridge to the northwest in the Southern Hemisphere. It appears that the strong westerlies just north of the equator were the result of the strong gradient between the relatively higher pressure to the west and the lower pressure to the east.

In summary, in the days prior to tropical cyclone genesis, there is very little evidence that the pressure perturbation from the South American anticyclone was strong enough to cause the westerlies just north of the equator (in fact there is no evidence that the perturbation ever crossed the equator). Therefore, while Love theorized that the enhanced westerlies were a result of pressure perturbation from the opposing hemisphere, it appears that in this case the strong westerlies just north of the equator were primarily the result of systems contained within the Northern Hemisphere. However, as shown in the previous section, the deepening in the equatorial trough was tied to the amplification of the Southern Hemisphere trough,

so indirectly the enhanced westerlies and subsequent tropical cyclone genesis can be at least partially attributed to the amplification of the Southern Hemisphere wave.

## V.3 Upper Level Diagnostics

A favorable wind flow in the upper levels is critical for tropical cyclone genesis. It is well known that strong divergence aloft is a necessary for tropical cyclone genesis. Strong upper level divergence typically implies upward vertical motion; this enhances convection and the evolution of a Conditional Instability of the Second Kind (CISK) mechanism (Charney and Eliassen, 1964). CISK is widely believed to be the mechanism responsible for the development of tropical disturbances into tropical cyclones.

The wind field is composed of the rotational wind (approximately 90%) and the divergent wind (approximately 10%). In the tropics the divergent wind may increase to as high as 50% of the total wind in localized regions, however for most regions the total wind is a fair approximation of the rotational wind. The total wind and the divergent wind charts for the period 27 May−1 June have been produced. The total wind will first be discussed.

### V.3.1 The 200 mb Wind and Streamlines

The 200 mb wind was computed using the x and y wind components and hand drawn streamlines are superimposed on the total wind to clarify features. The 200 mb streamlines confirm Fortune and Kousky's findings of the strong amplification of the South American trough due to the superposition of a short wave on a long

wave trough. At 0000 UTC 27 May (Fig. 19) a trough is located off the east coast of Argentina, and a smaller trough is located off the northwest coast of Chile. At 1200 UTC 27 May and 0000 UTC 28 May the troughs amplify slightly, and at 1200 UTC 28 May they superimpose and appear as one rather broad trough (Fig. 20). By 1200 UTC 28 May the primary axis of the trough (region of maximum curvature) extends northwest across the southern portions of South America into the Pacific, west of northern Chile. Throughout the remainder of the period (29 May–1 June) the trough appears to narrow, intensify, and gradually push eastward (Fig. 21, Fig. 22, Fig. 23, Fig. 24). The strong anticyclone associated with the cold surge is nearly stationary off the coast of Chile from 27–30 May, and gradually intensifies until it becomes a closed circulation at 0000 UTC 30 May. On 31 May and 1 June the anticyclone moves eastward over South America.

To the north, in the eastern North Pacific, strong anticyclonic flow is prevalent throughout the period, coinciding with low OLR values seen in section V.1. Initially on 0000 UTC 27 May the anticyclone was located over the Bay of Panama. By 0000 UTC 28 May the anticyclone moved to the northeast and greatly expanded. From 29–31 May the anticyclone gradually moves eastward and intensifies and strong cross-equatorial flow occurs between the two hemispheres. Strong divergent outflow is clearly evident in the southeastern and eastern sectors of the anticyclone. The presence of this 200 mb anticyclone over the eastern North Pacific appears to have assisted in providing a favorable environment necessary for tropical cyclone genesis.

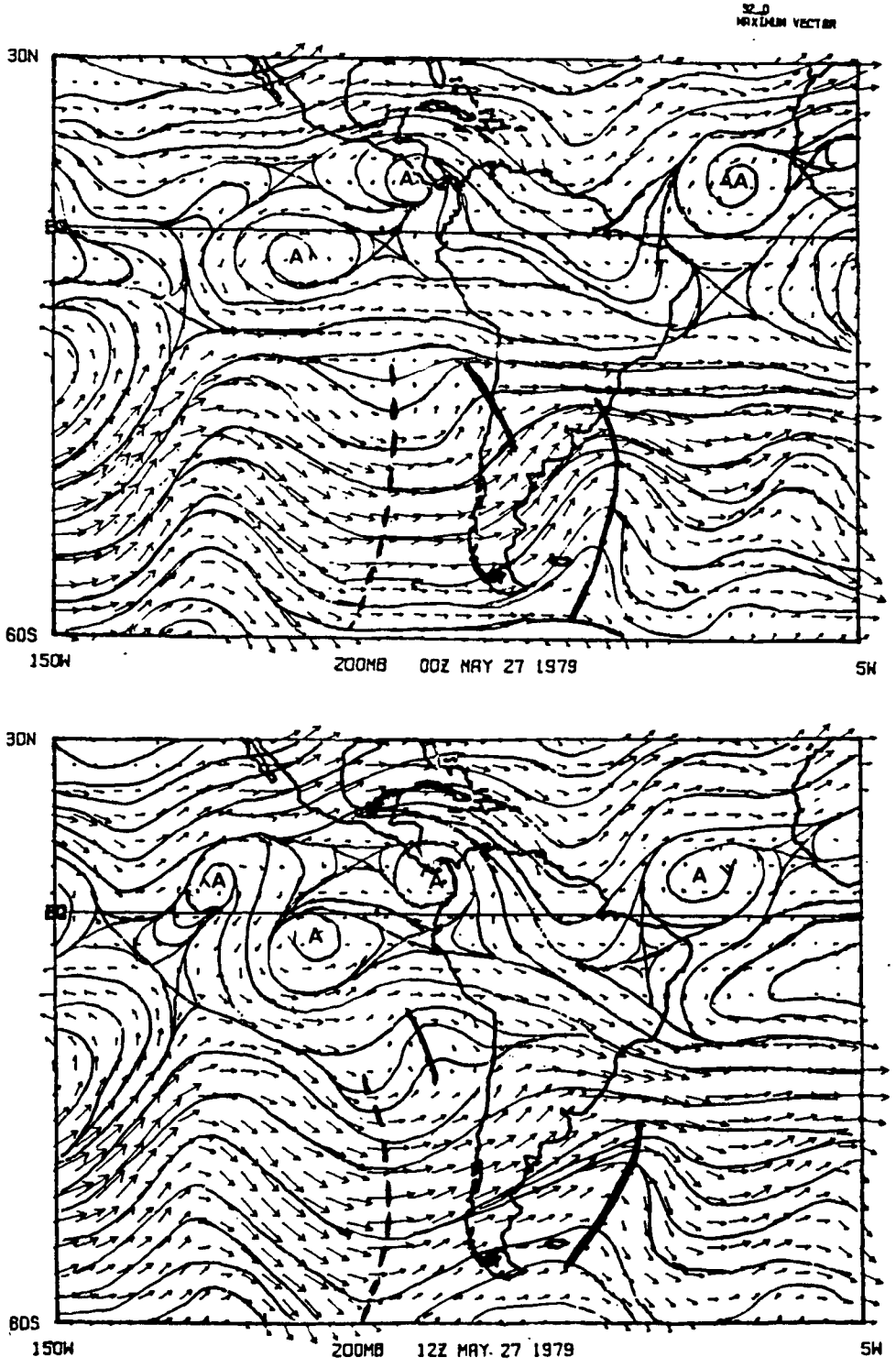


Figure 19. 200 mb winds for 27 May. Wind vectors are shown as arrows (reference vector is 32 m/s) and streamlines are shown as solid lines at 0000 UTC (top) and 1200 UTC (bottom). Solid heavy lines represent troughs and broken heavy lines represent ridges.

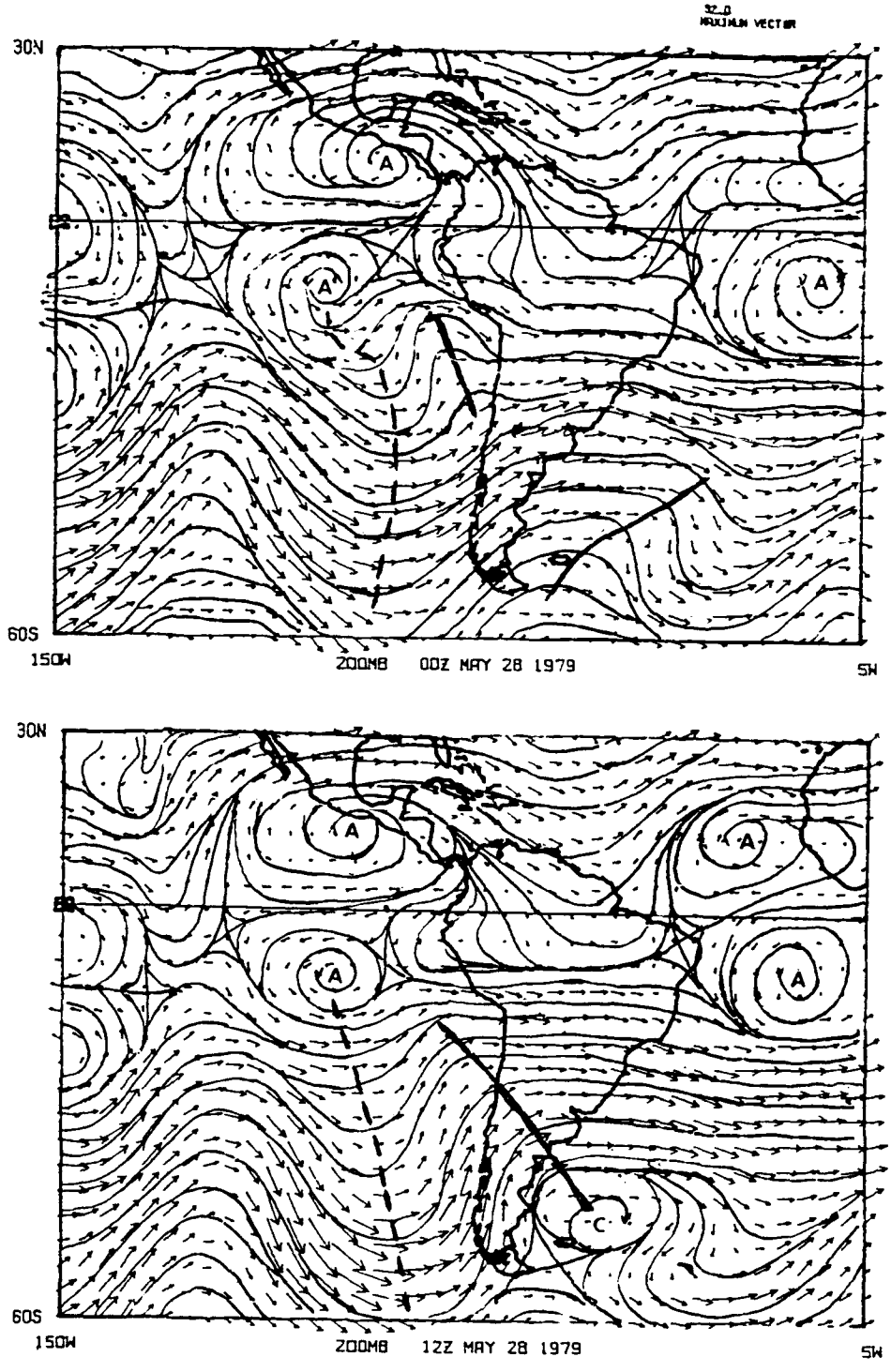


Figure 20. 200 mb winds for 28 May. Wind vectors are shown as arrows (reference vector is 32 m/s) and streamlines are shown as solid lines at 0000 UTC (top) and 1200 UTC (bottom). Solid heavy lines represent troughs and broken heavy lines represent ridges.

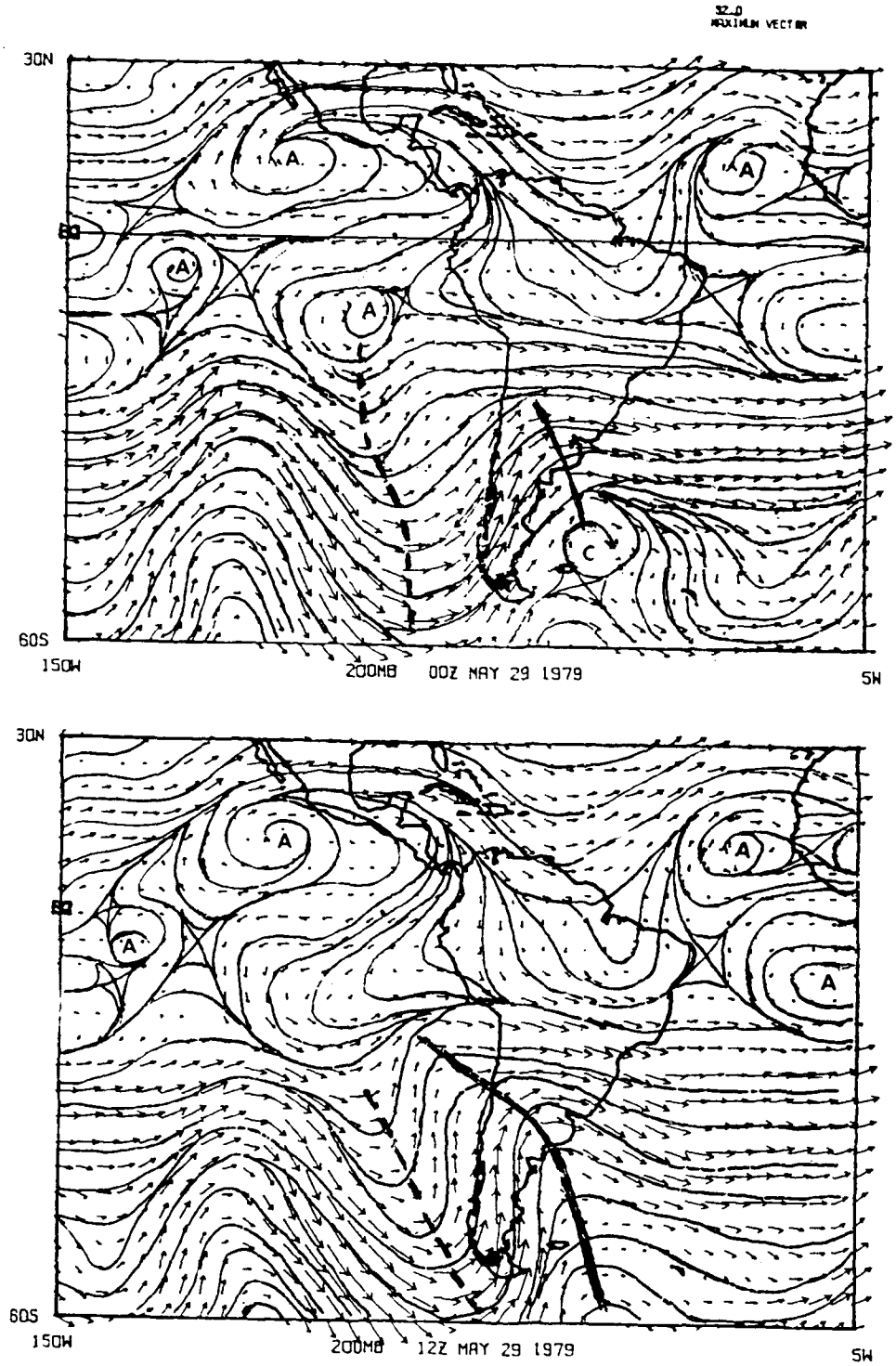


Figure 21. 200 mb winds for 29 May. Wind vectors are shown as arrows (reference vector is 32 m/s) and streamlines are shown as solid lines at 0000 UTC (top) and 1200 UTC (bottom). Solid heavy lines represent troughs and broken heavy lines represent ridges.

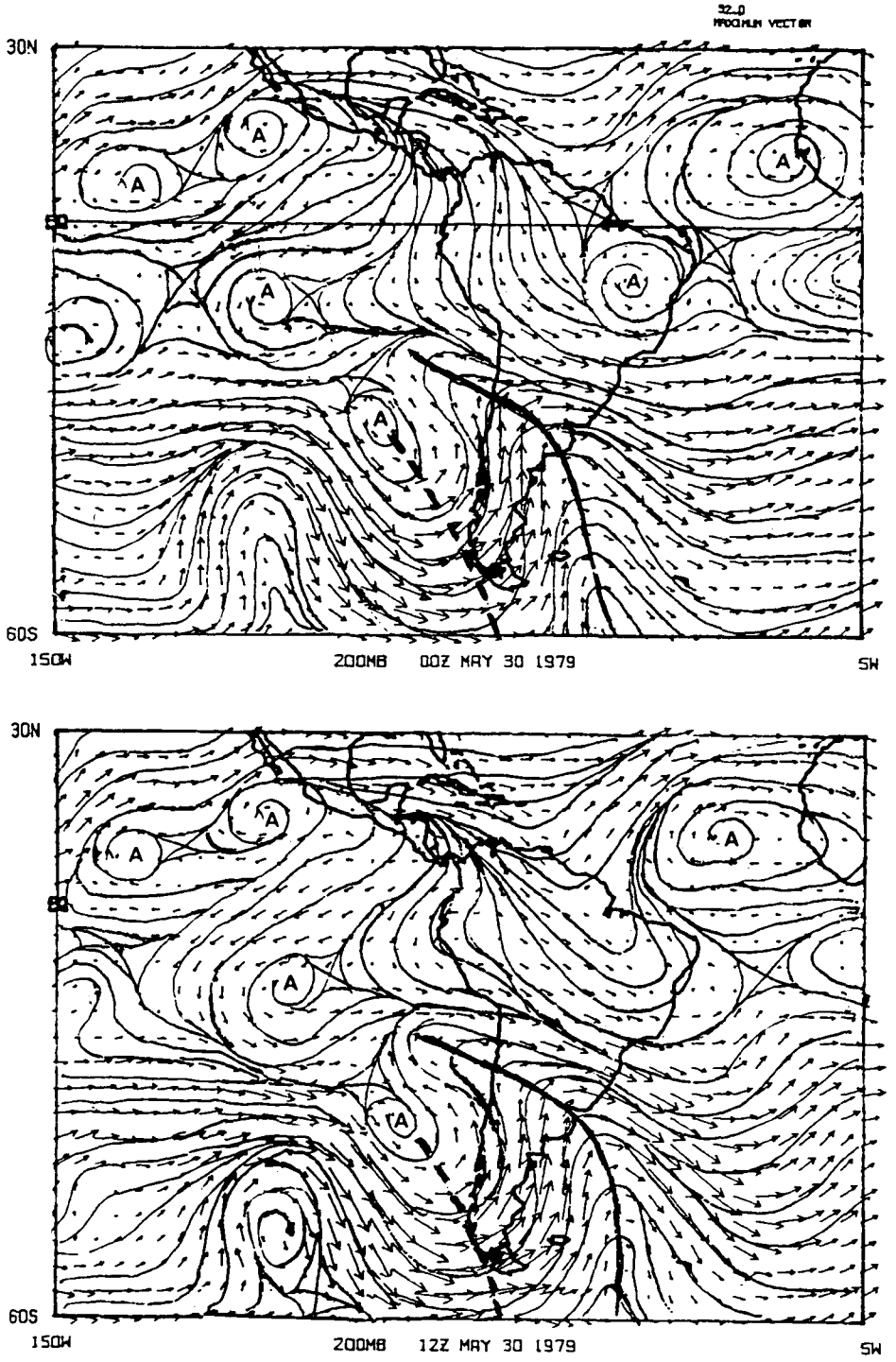


Figure 22. 200 mb winds for 30 May. Wind vectors are shown as arrows (reference vector is 32 m/s) and streamlines are shown as solid lines at 0000 UTC (top) and 1200 UTC (bottom). Solid heavy lines represent troughs and broken heavy lines represent ridges.

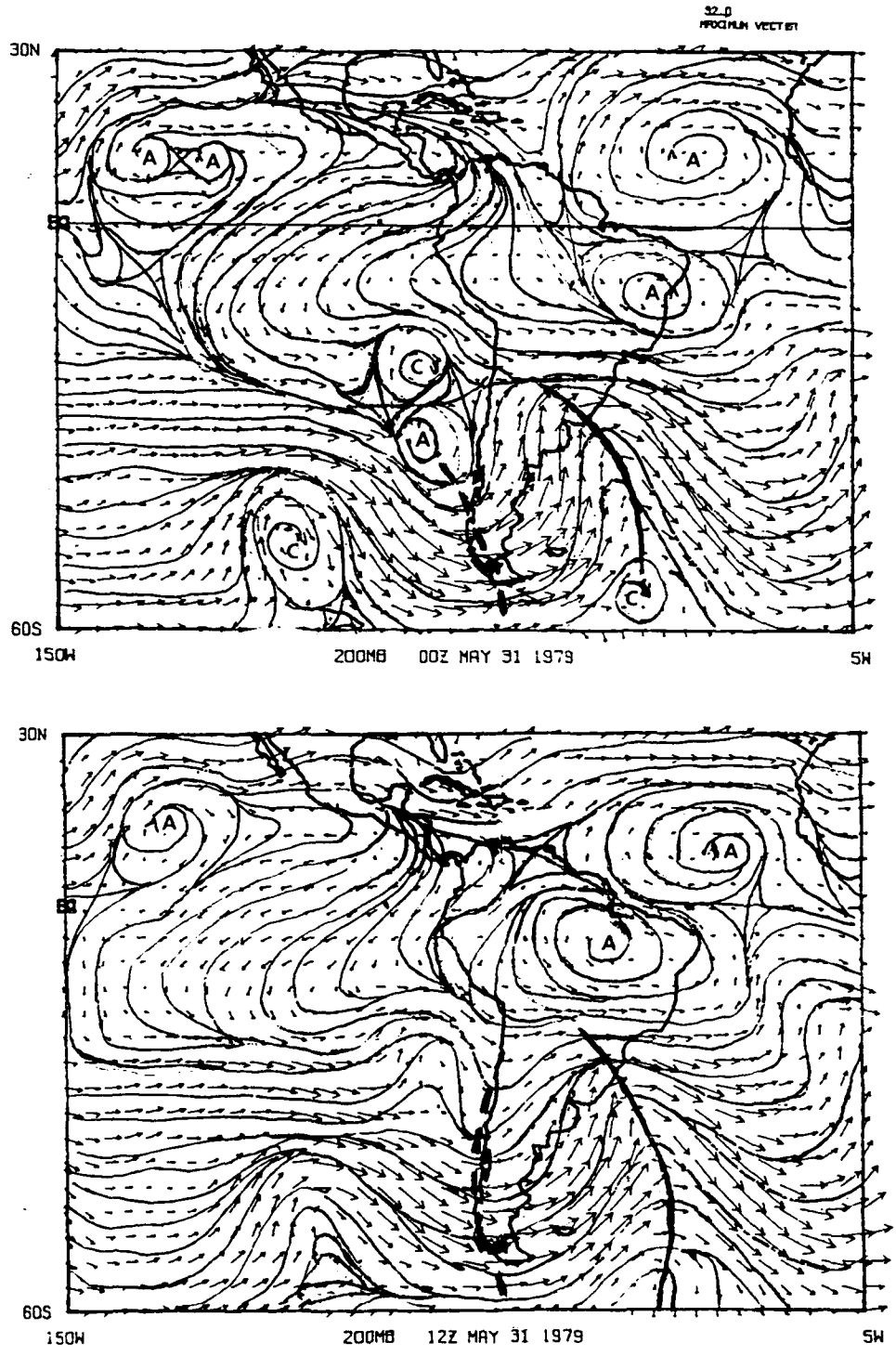


Figure 23. 200 mb winds for 31 May. Wind vectors are shown as arrows (reference vector is 32 m/s) and streamlines are shown as solid lines at 0000 UTC (top) and 1200 UTC (bottom). Solid heavy lines represent troughs and broken heavy lines represent ridges.

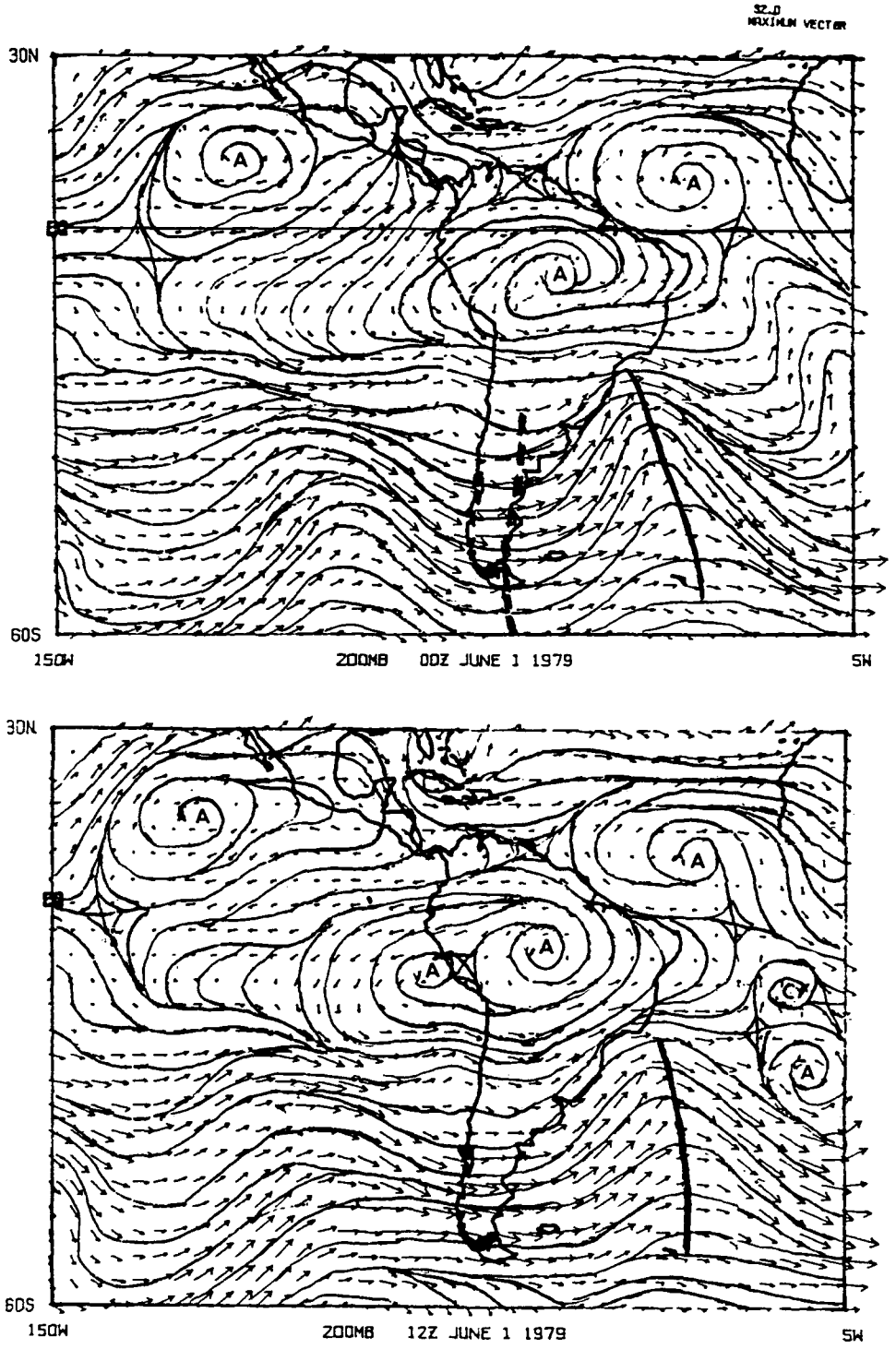


Figure 24. 200 mb winds for 1 June. Wind vectors are shown as arrows (reference vector is 32 m/s) and streamlines are shown as solid lines at 0000 UTC (top) and 1200 UTC (bottom). Solid heavy lines represent troughs and broken heavy lines represent ridges.

V.3.2 200 mb Divergent Wind

The 850 mb divergent wind was calculated from the x and y wind components for 27 May to 1 June. The divergence at each grid point was computed using the divergence definition:

$$D = \frac{\partial u}{\partial x} + \frac{\partial (v cos\theta)}{cos\theta \partial y}$$

The velocity potential ($\chi$ field) was then calculated from the divergence using the following formula:

$$D = \nabla^2 \chi$$

where the boundary conditions along the domain perimeter (section II.1, Fig. 1) were set to zero. The above equation was solved numerically using simultaneous relaxation. The initial guess was entered into the equation and solved for a remainder, then the remainder was used to obtain the next guess and the iteration continued until the remainder vanished and a solution was obtained. Since boundary values were prescribed as zero, the $\chi$ values near the boundary of the region should be regarded as estimates. The most accurate $\chi$ values are those in the center of the domain. Zonal and meridional divergent wind components were then computed using the following equations:

$$-u_\chi = \frac{\partial \chi}{\partial y}$$

$$v_\chi = \frac{\partial \chi}{\partial x}$$

The fields were calculated at 12 hour intervals for the period, and for. All times are shown in Figs.18–23. The fields were fairly slow changing; therefore, only the 0000 UTC period will be discussed.

At 0000 UTC 27 MAY (Fig. 25) the divergent wind was weak relative to the remainder of the period. The outflow associated with the 200 mb anticyclone in the eastern Equatorial Pacific is strongest in the northeastern quadrant over Central America. Weak convergence associated with the developing ridges is seen behind the mid-latitude troughs in the vicinity of Chile and Argentina. On 0000 UTC 28 May (Fig. 26) there is a large amplification of the divergent wind. The anticyclone aloft over the eastern Equatorial Pacific rapidly develops and the majority of the outflow is now directed to the north and south. The southward directed outflow converges into the northern portion of the Southern Hemisphere ridge off the northern coast of Peru. The line of convergence associated with the subtropical ridge is located off the west coast of South America and extends from Peru to Chile. In the following days the convergence intensifies indicating a strengthening of the Southern Hemisphere ridge, not only from the large mass influx from the subsiding outflow from the eastern Equatorial Pacific anticyclone, but also due to the converging outflow of the mid-latitude troughs to the west and east of the ridge. A strong local meridional overturning is emerging rapidly between the equatorial trough region and the Southern Hemisphere ridge. The amplification continues

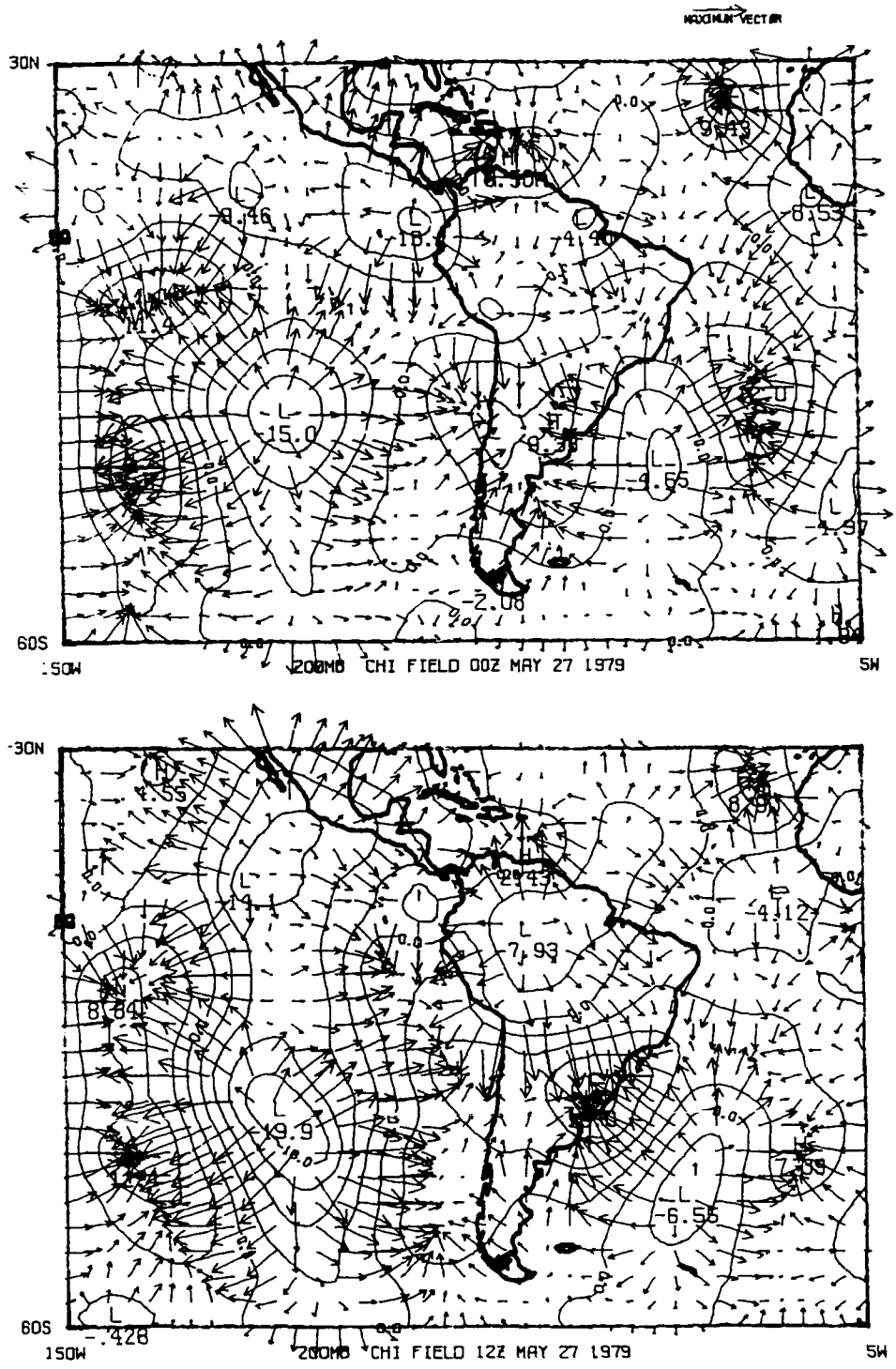


Figure 25. 200 mb divergent wind and velocity potential for 27 May. The divergent wind are shown as vectors (reference vector is 2.5 m/s), and the velocity potential are solid lines (4 x $10^5$ $m^2/s$ intervals) at 0000 UTC (top) and 1200 UTC (bottom).

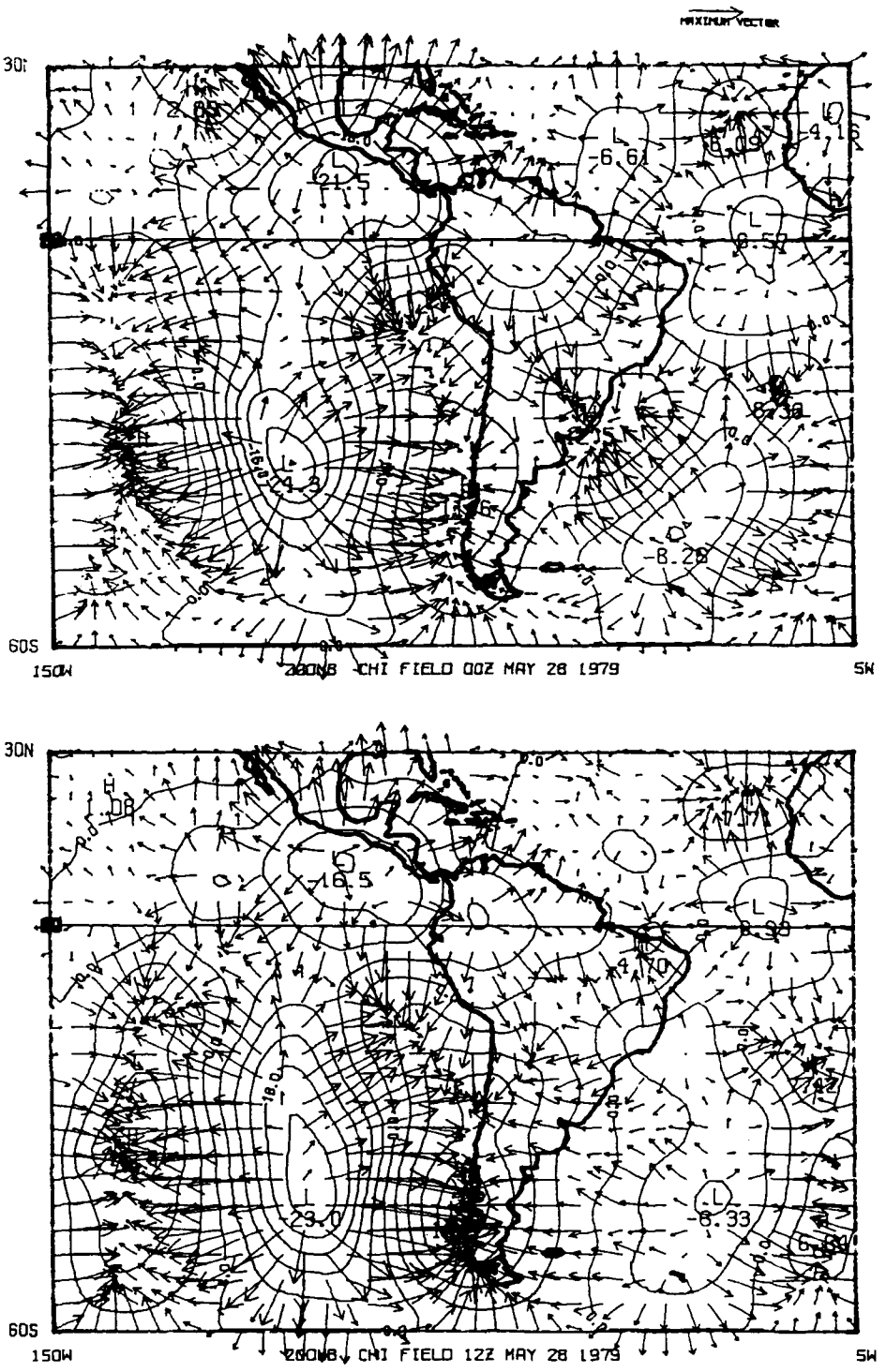


Figure 26. 200 mb divergent wind and velocity potential for 28 May. The divergent wind are shown as vectors (reference vector is 2.5 m/s), and the velocity potential are solid lines (4 x $10^5$ $m^2/s$ intervals) at 0000 UTC (top) and 1200 UTC (bottom).

at 0000 UTC 29 May, as the localized meridional overturning further strengthens (Fig. 27). There is little change in the minimum velocity potential over the eastern Equatorial Pacific, however the region of outflow has greatly expanded. The outflow now appears to be strongest to the south of the eastern Equatorial anticyclone, where the strong Southern Hemisphere ridge behind the frontal band continues to provide a sink for it. At 0000 UTC 30 May, one day before the Southern Hemisphere front seems to be strongest (Chapt. IV), there is an enormous decrease in the velocity potential (strong divergence) north-northeast of the Falkland Islands, over 300% in 24 hours (Fig. 28). The velocity potential in the eastern Equatorial Pacific continue to increase and strong divergent outflow further intensifies the Southern Hemisphere ridge. By 0000 UTC 31 May (Fig. 29) the surface front is in Central Brazil. The upper level convergence behind the front moves to the northeast over the Uruguay coast, breaking off somewhat from the ridge axis The convergence associated with the subtropical ridge to the west seems to be weakening. Divergent outflow from the eastern Equatorial Pacific is still very strong indicating the equatorial trough is exceptionally active. By 0000 UTC 1 June (Fig. 30) the tropical cyclones have formed and the cold surge in Brazil has occurred. The inter-hemispheric meridional overturning is rapidly weakening as the Southern Hemisphere front pushes eastward and looses strength.

The 200 mb divergent wind analyses reveal that as the Southern Hemisphere wave amplified, there was an enormous amplification in the local meridional overturning, which advected mass out of the equatorial North Pacific and into the anticyclone

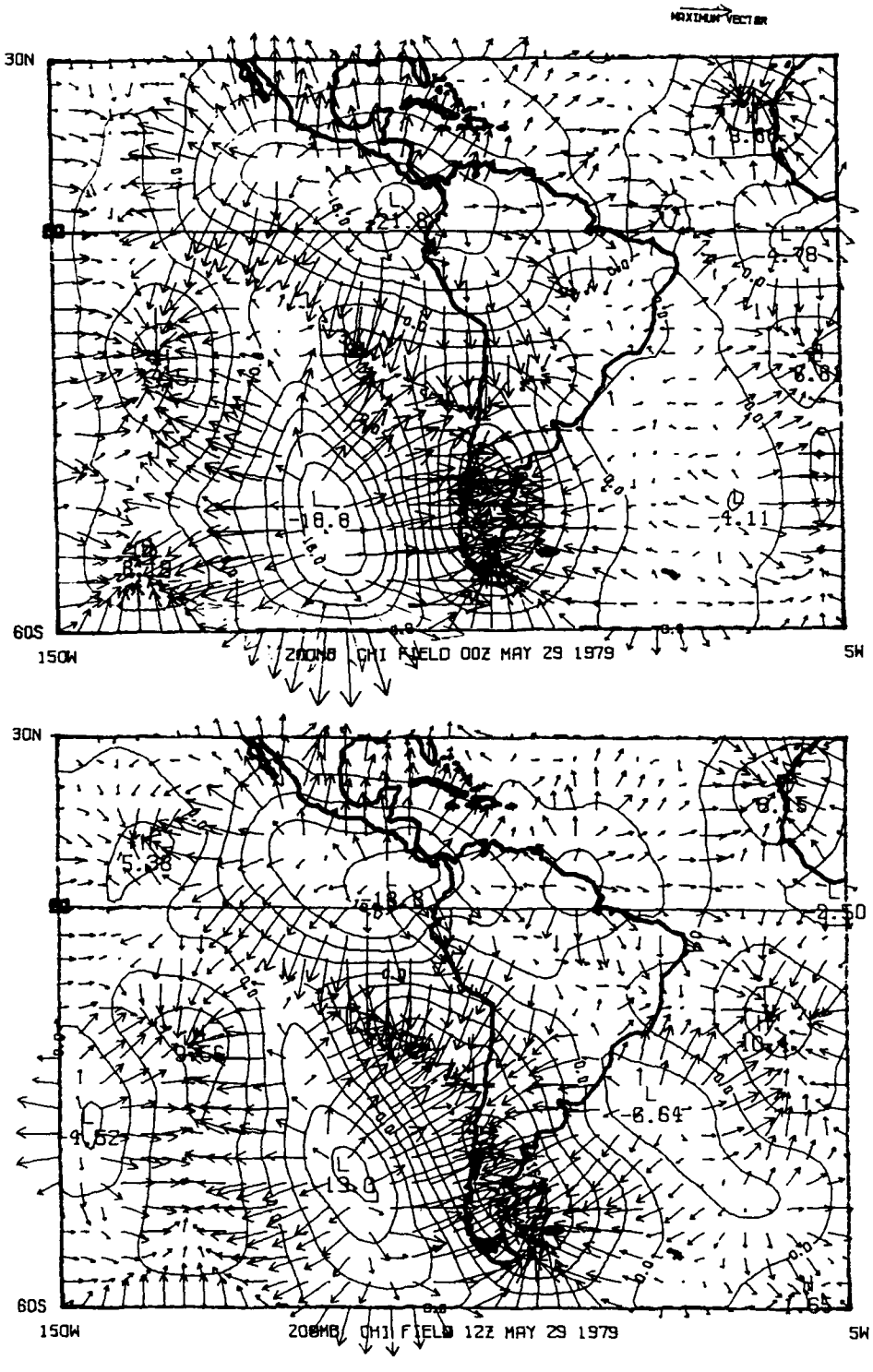


Figure 27. 200 mb divergent wind and velocity potential for 29 May. The divergent wind are shown as vectors (reference vector is 2.5 m/s), and the velocity potential are solid lines (4 x $10^5$ $m^2/s$ intervals) at 0000 UTC (top) and 1200 UTC (bottom).

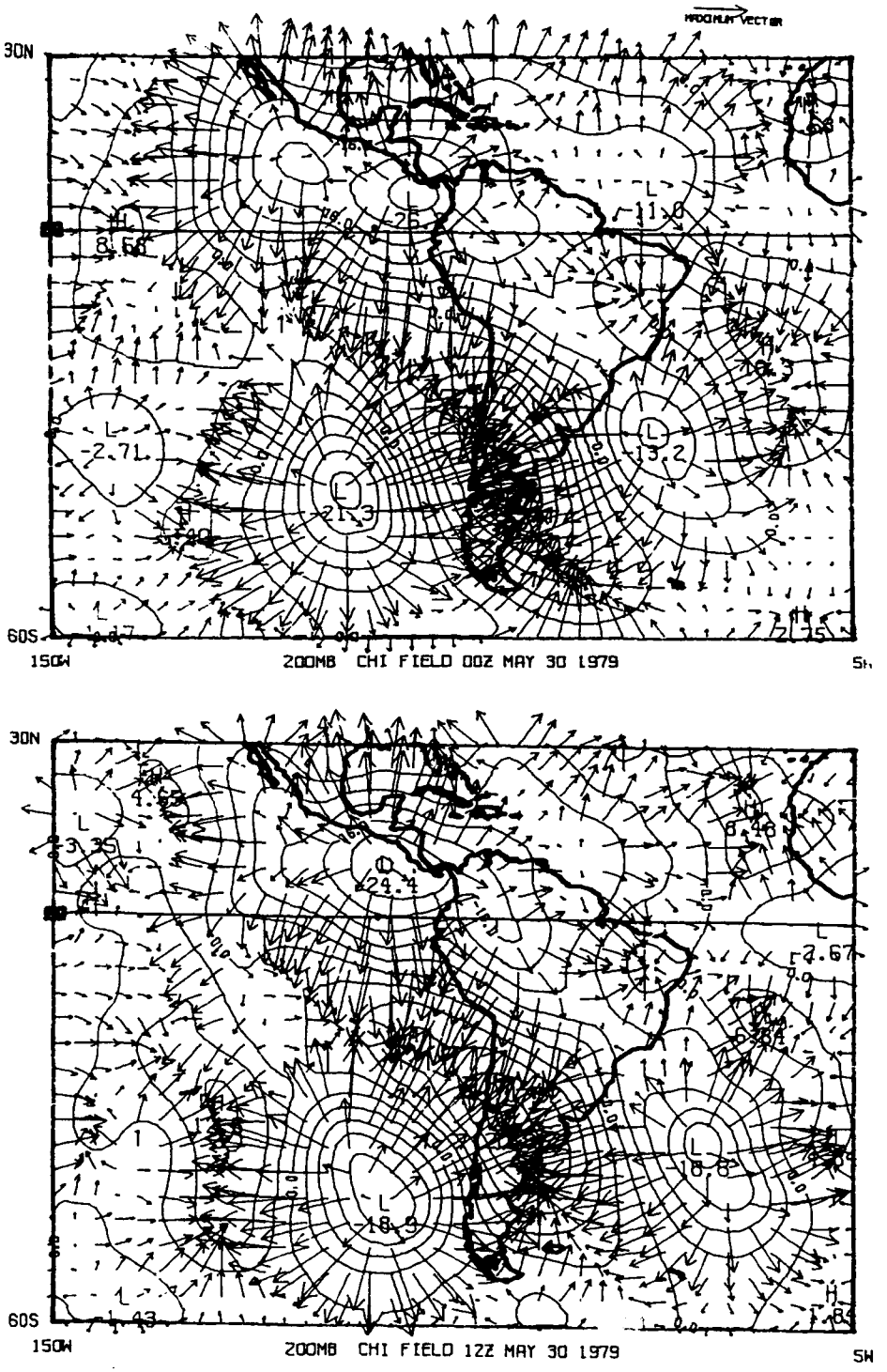


Figure 28. 200 mb divergent wind and velocity potential for 30 May. The divergent wind are shown as vectors (reference vector is 2.5 m/s), and the velocity potential are solid lines (4 x $10^5$ $m^2/s$ intervals) at 0000 UTC (top) and 1200 UTC (bottom).

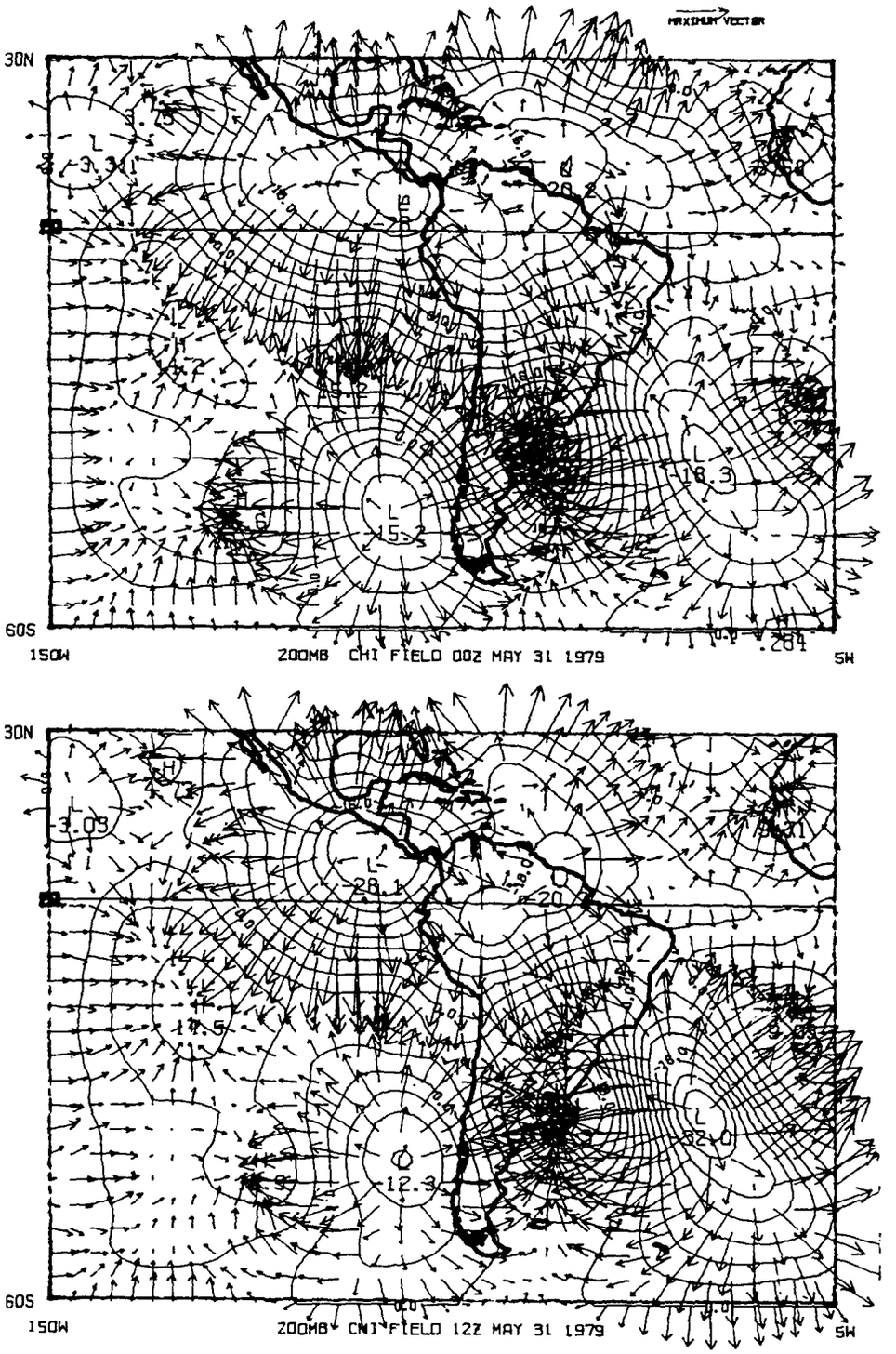


Figure 29. 200 mb divergent wind and velocity potential for 31 May. The divergent wind are shown as vectors (reference vector is 2.5 m/s), and the velocity potential are solid lines (4 x $10^5$ $m^2/s$ intervals) at 0000 UTC (top) and 1200 UTC (bottom).

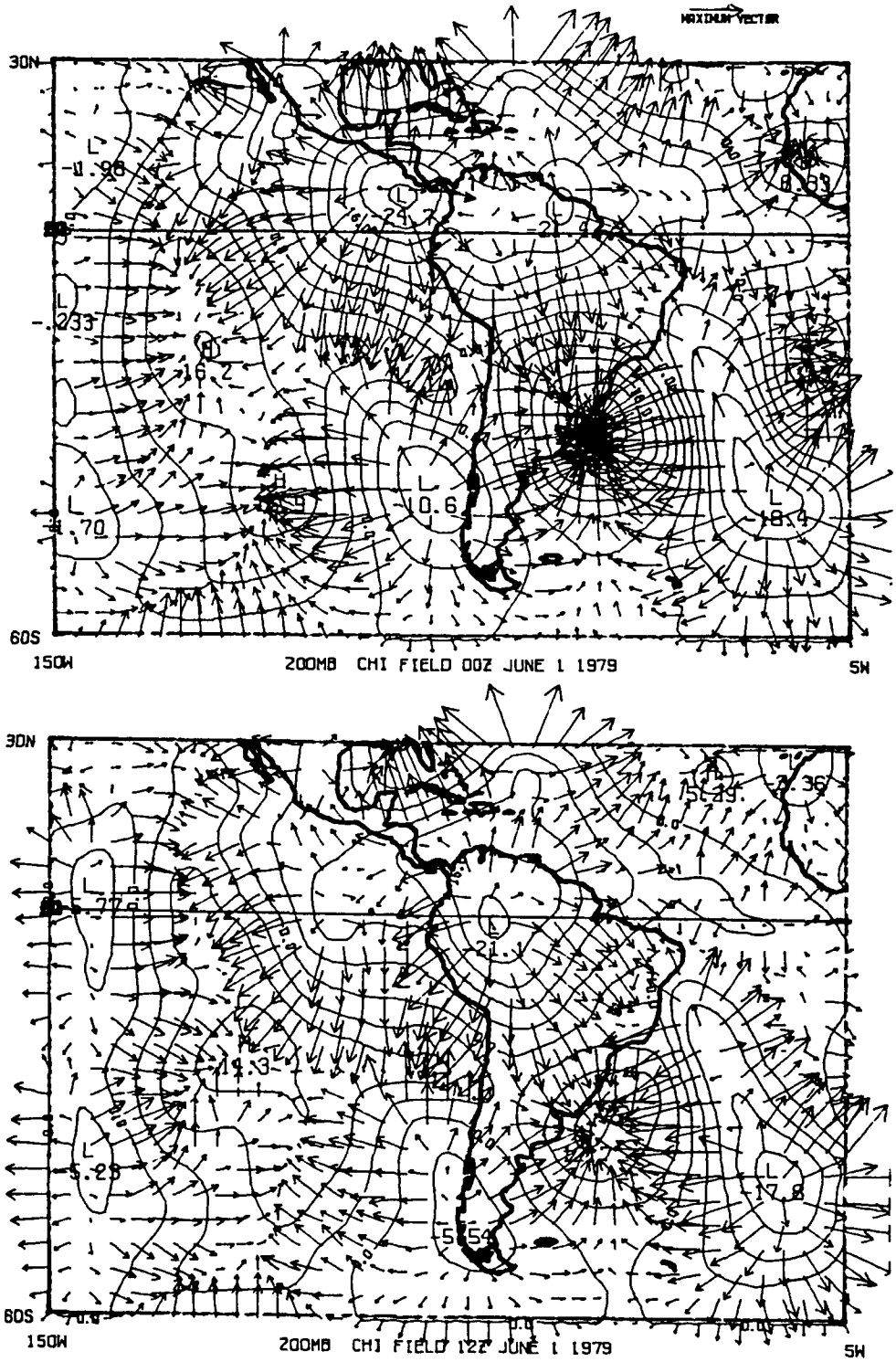


Figure 30. 200 mb divergent wind and velocity potential for 1 June. The divergent wind are shown as vectors (reference vector is 2.5 m/s), and the velocity potential are solid lines (4 x $10^5$ $m^2/s$ intervals) at 0000 UTC (top) and 1200 UTC (bottom).

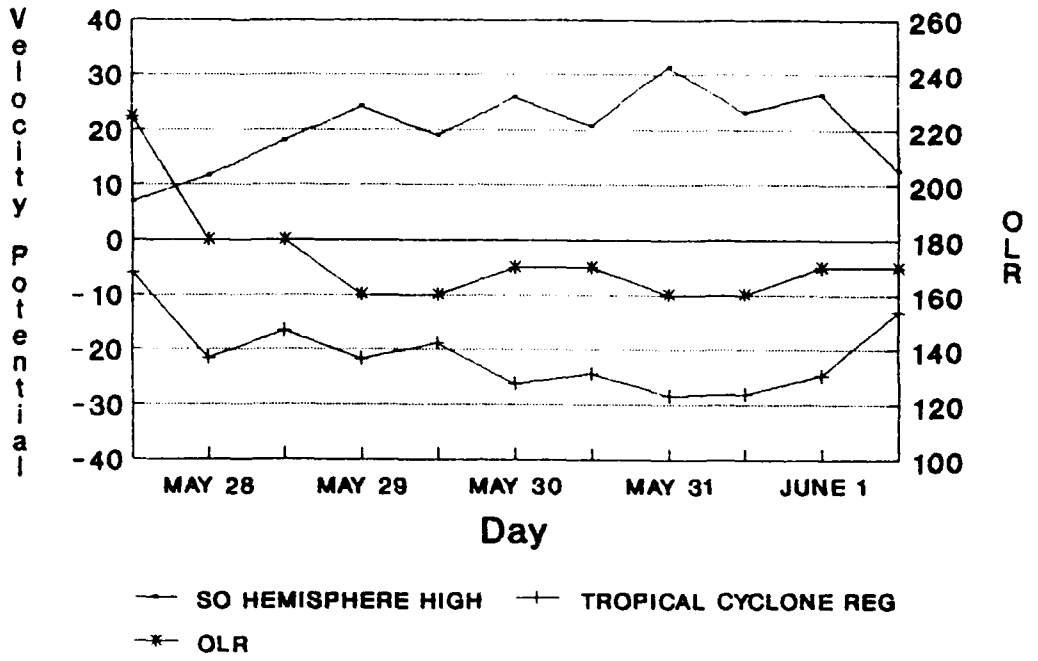


Figure 31. Time series of velocity potential and OLR. Maximum values of velocity potential over the Southern Hemisphere anticyclone, minimum values of velocity potential (1 x $10^5$ $m^2/s$) in the region of tropical cyclone genesis for 27 May–1 June at 0000 UTC and 1200 UTC are plotted. Daily averages of the minimum OLR values ($W/m^2$) in the region of tropical cyclone are also plotted.

the cross-equatorial tie is between these two systems, the minimum velocity potential in the region of tropical cyclone genesis was plotted against the maximum velocity potential over the Southern Hemisphere anticyclone from 28 May to 1 June at 0000 UTC and 1200 UTC (Fig. 31) . The plots are nearly mirror images of one another, the velocity potentials in both systems intensify and weaken in unison. The maximum intensity of the velocity potentials of both systems occurs on 31 May, the same day the freeze occurred in Brazil and the two tropical cyclones developed in the eastern

the freeze occurred in Brazil and the two tropical cyclones developed in the eastern Equatorial Pacific. It is interesting that the intensification of one system does not seem to proceed the other, thus indicating the initial source of strengthening of the systems may not necessarily be associated with the other system but rather from an external source. This leads one to believe a downstream propagation of energy may be responsible for the initial intensification in the divergent wind of these systems (see Chapt. VI). The maximum OLR value over the region of minimum velocity potential was also plotted. As the velocity potential decreases, the OLR should also decrease in response to the increased vertical motion. The OLR strongly decreases between 27/1200 UTC and 0000 UTC 28 May in conjunction with the decrease in velocity potential. For the remainder of the period the OLR values remain low and closely mimic the velocity potential curve in the region of tropical cyclone genesis, confirming strong upper level divergence in the region.

Thus, it is clear there is a strong inter-hemispheric interaction between the two systems in the upper levels through the intensification of the divergent wind and strong amplification of the meridional overturning. This interaction first appeared between 1200 UTC 27 May and 0000 UTC 28 May and intensified until tropical cyclone genesis occurred at 1800 UTC 31 May. This strong localized meridional overturning served to deepen the equatorial trough as well as strengthen the subtropical ridge behind the frontal band.

# CHAPTER VI

## LARGE SCALE DIAGNOSTICS

The large scale circulation appears to play a major role in the amplification of the ridge-trough system over South America. Rossby (1949) demonstrated that strong wave amplification is a result of the downstream transfer of energy through dispersive waves. Since wave energy travels faster than the wave itself, a strong remote perturbation will propagate quickly downstream in the westerlies, well ahead of the actual wave. Hovmöller (1949) developed a diagram to illustrate wave phase and energy propagation. For a fixed latitude, he plotted time on the vertical axis against longitude on the horizontal axis. Fortune and Kousky (1983) in a similar manner plotted the 1000−500mb thickness values at 28°S extending from 15°W to 140°W. While Hovmöller diagrams at a single degree latitude do not tell the entire story, they do give a good indication of the downstream propagation of the energy at a particular latitude band.

To illustrate the Southern Hemisphere propagation more clearly, Fortune and Kousky's Hovmöller diagrams have been reconstructed in this study to encompass an entire latitude band around the globe at 28°S using geopotential height deviations for the 200, 500 and 850mb levels. The mean global geopotential heights at 28°S for 26 May−1 June at 0000 UTC and 1200 UTC were calculated at each level and subtracted from the value at each grid point along 28°S at that level to get the geopotential height

deviation. This height deviation is plotted as a function of longitude and time for each level (Fig. 32) .

The propagation first appears on 26 May at 140°W. Unfortunately, due to the restrictions of the data set (lack of data before 26 May) it is impossible to specify the exact source region of the propagation. The wave energy propagates downstream at a group velocity of approximately 35°–40° longitude per day. The amplification begins to appear in the South American region on 27 May. On 29 and 30 May the wave sharply amplifies at all levels, corresponding to the passage of the wave energy over South America. This strong amplification of the ridge–trough system is what ultimately results in the cold surge in Southern Brazil on 31 May and appears to have been influential in the formation of the tropical cyclones in the eastern North Pacific. The energy packet continues to propagate around the earth at 28°S until it reaches Greenwich meridian on 31 May, at which time the propagation breaks down.

The wave is most intense in the upper layers and gradually weakens downward (Fig. 32). In the Eastern Hemisphere the wave is nearly vertically stacked, indicating the atmosphere is equivalent barotropic in this region. However, in the Western Hemisphere the atmosphere is baroclinic, as would be expected for a propagating wave associated with a developing system. The South American wave is tilted most between the 850 mb and 500 mb levels (approximately 350 km tilt to the west with height), and nearly vertically stacked between 500 mb and 200 mb.

The wavelength of the ridge–trough system over South America is approximately 60°–70° which corresponds to wave number 5 or 6. In an effort to discover

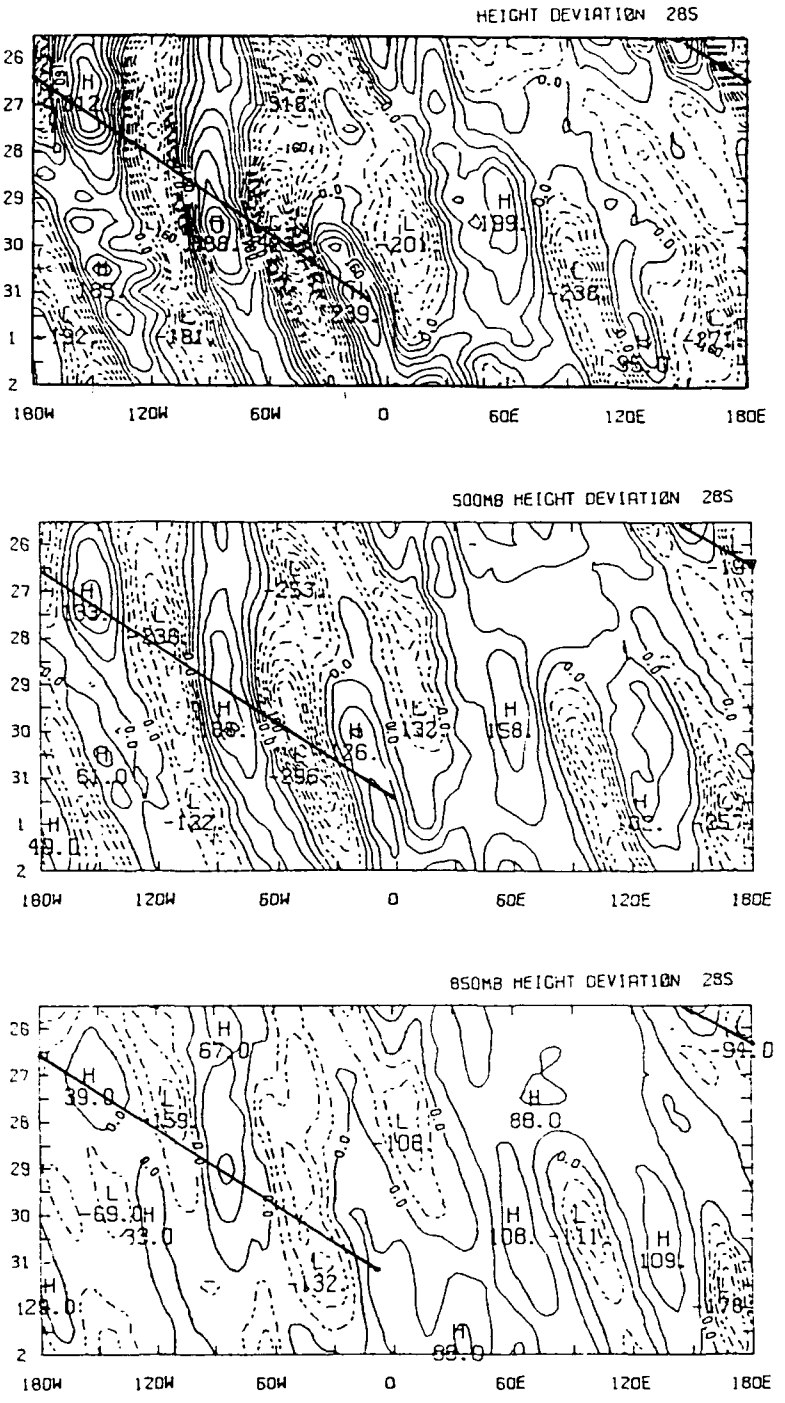


Figure 32. Geopotential height deviation from zonal mean at 28°S. The geopotential height is plotted as a function of longitude (horizontal axis) and day (vertical axis) for 200 mb (top), 500 mb (middle) and 850 mb (bottom) with contour intervals of 40 gpm.

how much of total field can be explained by these waves, a Fourier analysis was done using 200 mb geopotential heights.

$$F_i = \frac{a_o}{2} + \sum_{n=1}^{95} C_n cos[\frac{2\pi\eta}{I}(i-1) - \phi_n]$$

where

$$C_n = \left(a^2{}_n + b^2{}_n\right)^{1/2}$$

and

$$\phi_n = tan^{-1}(b_n/a_n)$$

with

$$a_n = \frac{2}{I}\sum_{i=1}^{I} F_i cos\frac{2\pi n}{I}(i-1)$$

$$b_n = \frac{2}{I}\sum_{i=1}^{I} F_i sin\frac{2\pi n}{I}(i-1)$$

where $F_i$ is the value of the function at interval $i$, $a_o$ is the mean $\phi$ along 28°S, $C_n$ is the wave amplitude coefficient, $a_n$ is the cosine component of the wave coefficient and $b_n$ is the sine component of the wave coefficient, $n$ is the wave number, $I$ is the number of grid intervals, and $\phi_n$ is phase between the wave maximum and the origin.

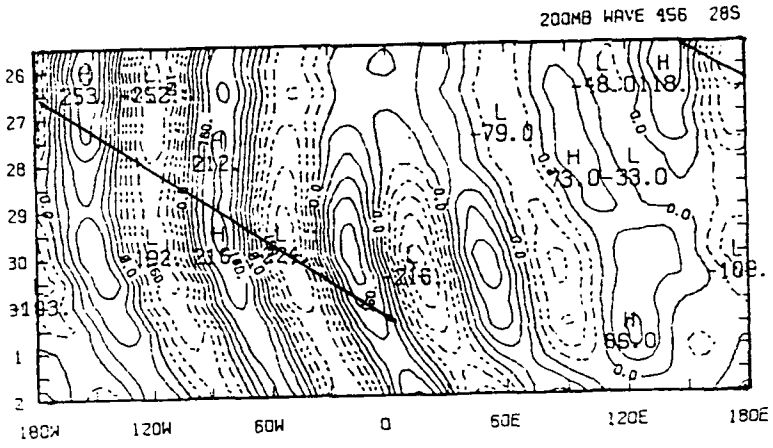


*Figure 33. 200 mb geopotential height deviation at 200 mb for the sum of wave numbers 4, 5, and 6. The geopotential height is plotted as a function of longitude (horizontal axis) and day (vertical axis)with contour intervals of 40 gpm.*

After trying various 3-wave combinations of wave numbers 3, 4, 5, 6, and 7, the sum of wave numbers 4, 5, and 6 resembled best the total 200 mb geopotential height deviation (Fig. 33) .

As 96 waves numbers can be resolved in this data set, it is remarkable that a combination of only three resembles the total field so well. In fact approximately 53% of the total deviation on 29 May at 28°S over South America can be explained by these three waves.

Individually, wave numbers 4, 5, and 6 resemble the total field much less (Fig. 34). Wave numbers 5 and 6 are very strong compared to wave number 4. All three waves are nearly stationary or slightly retrogressive from 26 to 28 May. At 1200 UTC on 28 May wave numbers 5 and 6 begin to amplify, while wave number 4 decreases in amplitude and goes to zero at 1200 UTC 29 May. Strongest amplification of wave numbers 5 and 6 occurs between 29 and 31 May, and constructive interference of these waves over South America are responsible for the overall strong amplification. Once wave numbers 5 and 6 begin amplifying at 1200 UTC 28 May they also begin to propagate eastward. The addition of wave number 4, though very weak, allows for the subtle variations regarding the continuous propagation of the wave downstream.

In chapt. V it was shown that the large amplitude of the southern wave and the amplification of the localized meridional overturning appeared to be influential in the development of the two tropical cyclones in the eastern equatorial Pacific. The strengthening of the meridional overturning was first observed at 1200 UTC 27 May, the same time as the energy propagation began to appear in the South American region. The strong amplification of the Southern Hemisphere wave, which ultimately was very influential in increasing low-level vorticity in the eastern equatorial Pacific, occurred as the energy propagation was most strongly defined on 29 and 30 May. It therefore appears that the anomalous intensification of both the Southern Hemisphere wave and the increased activity over the eastern equatorial Pacific can be directly linked to the downstream propagation of energy which originated west of the date line before 26 May.

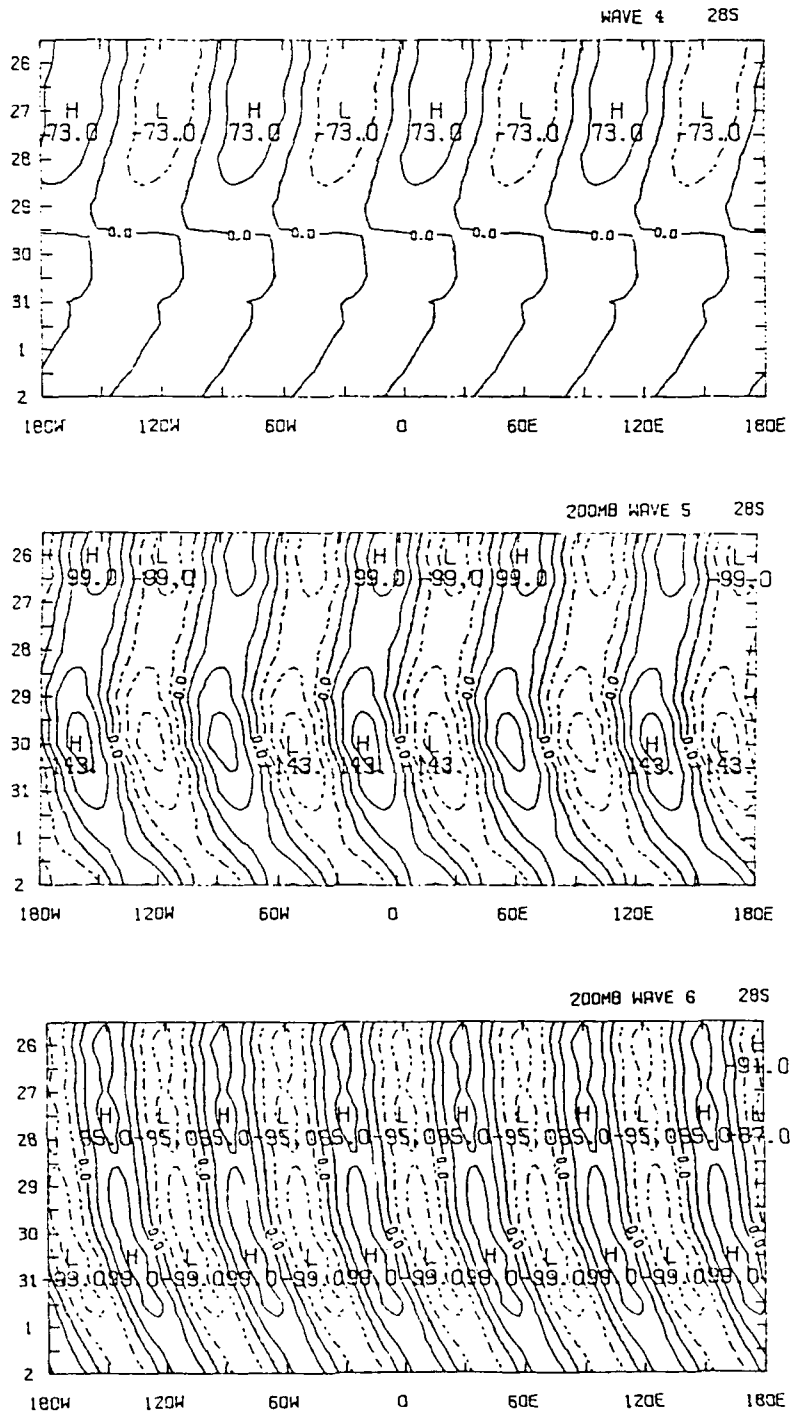


Figure 34. 200 mb geopotential height deviations for wave numbers 4, 5, and 6. The geopotential height is plotted as a function of longitude (horizontal axis) and day (vertical axis). Wave number 4 is shown on top, wave number 5 in middle, and wave number 6 at bottom with contour intervals of 40 gpm.

# CHAPTER VII

## SUMMARY AND DISCUSSION

The results of this research indicate that the large amplitude of the South American wave was instrumental in the formation of the tropical cyclones in the eastern Equatorial North Pacific, and that this unusually large amplitude was the result of the downstream propagation of energy contributed by the superposition of wave numbers 4, 5 and 6. The inter-hemispheric link between the cold surge and the development of tropical cyclones appeared to be associated with the rotational wind at low levels and with the divergent wind at upper levels.

At low levels the subtropical ridge was displaced north (nearly to the equator) of its normal position. The Southern Hemisphere wave strongly amplified and as the trough developed equatorward, it broke through the ridge, severing a small portion of the anticyclone from it. This eddy then moved into the Northern Hemisphere becoming a cyclone and merged with the equatorial trough (Fig. 35 ). The equatorial trough deepened, and along with the strengthening of a Northern Hemisphere anticyclone to the west, the large scale scale pressure gradient in the eastern Equatorial Pacific strengthened, and westerlies developed just north of the Equator. These westerlies increased the low level vorticity in the eastern North Pacific and set up a favorable environment for tropical cyclone genesis.

At the upper levels the inter-hemispheric interaction appeared to be strongly tied to the divergent wind. The 200 mb divergence in the eastern equatorial North Pacific was strong prior to the amplification of the Southern Hemisphere wave. However,

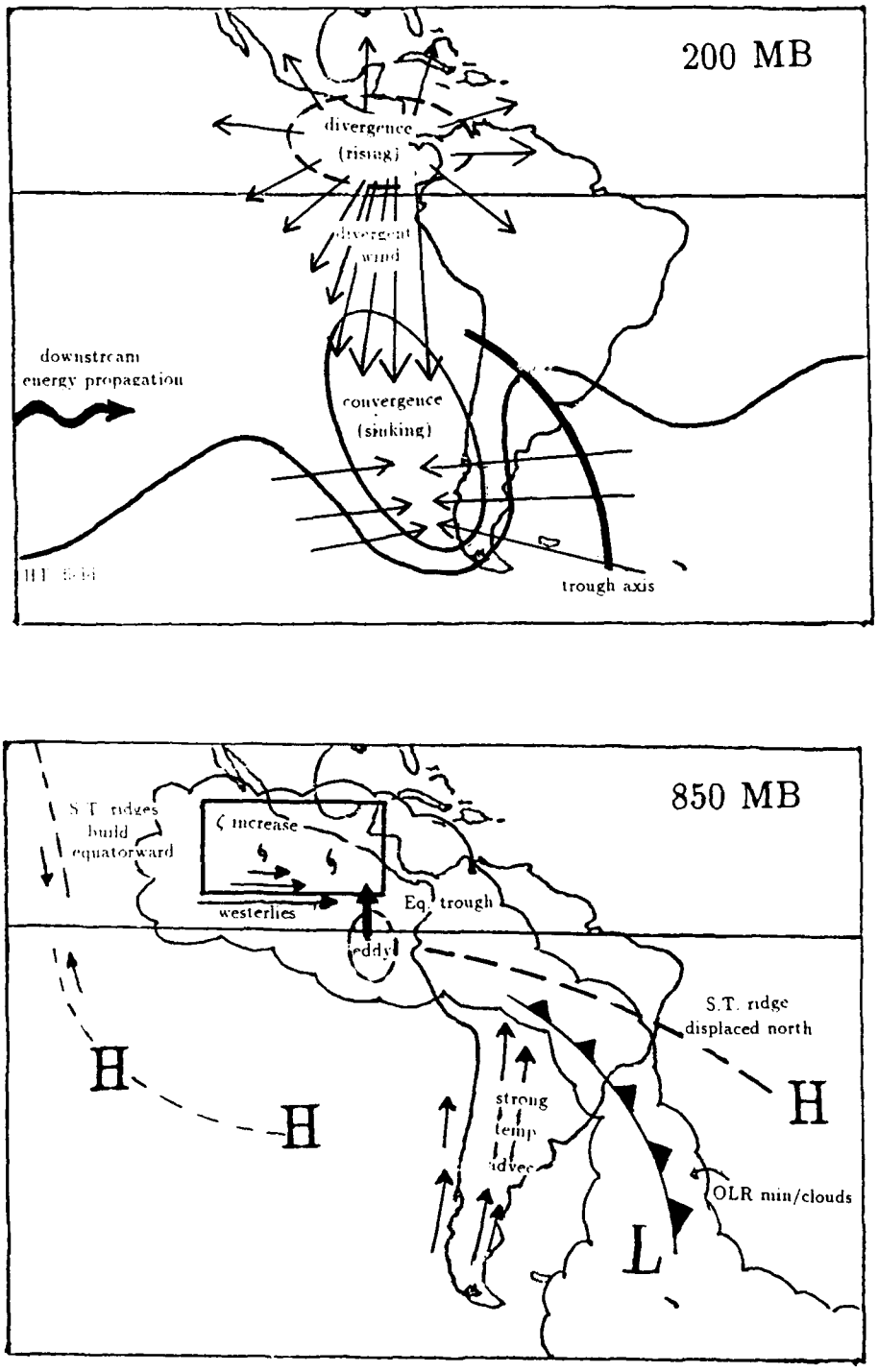


Figure 35. Schematic diagrams showing the positions of important features. The top diagram is at 200 mb and the bottom at 850 mb.

after amplification the upper level divergence greatly intensified, in what appeared to be an excitation of a local meridional overturning. The anticyclone behind the Southern Hemisphere trough provided a sink for the mass moving away from upper levels over the region of cyclone genesis, this enormous mass transport served to strengthen both systems (the Equatorial trough and the Southern Hemisphere anticyclone). The fact that the velocity potential of the systems increased and decreased in unison and that amplifications of both systems was also simultaneous (Fig. 30), indicates that one system did not "cause" the other system, but that they developed together, in what appeared to be a symbiotic relationship. The strengthening of both systems, and ultimate formation of the tropical cyclones, appeared to be directly tied to the enormous intensification in the upper branch of a localized meridional (Hadley) circulation which in turn appeared to be directly tied to the downstream propagation of energy originating in the west Pacific. The important features associated with this scenario is depicted in the schematic in Fig. 35.

Certainly, from one case study we cannot conclude that all tropical cyclones associated with cold surges form in this manner. Both events, the cold surge and the simultaneous formation of the two tropical cyclones were highly unusual events. Further study needs to be conducted on other tropical cyclone-cold surge events to determine if the cross-equatorial interactions identified in this study are common to other similar events.

# REFERENCES

Alaka, M. A., 1958: Dynamics of upper-air outflow in incipient hurricanes. *Geophysica*, **6**, 133-146.

Bengtsson, L., M. Kanamitsu, P. Kallberg, and S. Uppala, 1982: FGGE 4-dimentional Data Assimilation at ECMWF. *Bull. Amer. Meteor. Soc.*, **63**, 29-43.

Charney, J. C. and A. Eliassen, 1964: On the growth of the hurricane depression. *J. Atmos. Sci.*, **21**, 68-75.

Chu, P. S., 1986: Tropospheric circulation associated with a cold surge event in South America during southern winter. Extended abstracts, Second International Conference on Southern Hemisphere Meteorology AMS, 52-55.

Fortune, M. A. and V. E. Kousky 1983: Two severe freezes in Brazil: precursors and synoptic evolution. *Mon. Wea. Rev.* **111**, 181-196.

Gray, W. M., 1968: Global view of the origin of tropical disturbances and storms. *Mon. Wea. Rev.* **96**, 669-700.

——, 1975: Tropical cyclone genesis. Paper No. 234, Dept. of Atmos. Sci., Colorado State Univ., Fort Collins.

Gruber, A. and J. S. Winston 1978: Earth-atmosphere radiative heating based on NOAA scanning radiometer measurements. *Bull. Amer. Meteor. Soc*, **59**, 1570-1573.

——, and A. F. Krueger 1984: The status of the NOAA outgoing longwave radiation data set. *Bull. Amer. Meteor. Soc*, **65**, 958-962.

Gunther, E. B. 1980: Eastern North Pacific tropical cyclones of 1979. *Mon. Wea. Rev.* **108**, 631-641.

Hovmöller, E. 1949: The trough ridge diagram. *Tellus* **1**, 62-66.

Love, G., 1982: The Role of general circulation in Western Pacific tropical cyclone genesis. Paper No. 340, Dept. of Atmos. Sci., Colorado State Univ., Fort Collins.

——, 1985a: Cross-equatorial influence of winter hemisphere subtropical cold surges. *Mon. Wea. Rev.* **113**, 1487-1498.

—, 1985b: Cross-equatorial interactions during tropical cyclonegenesis. *Mon. Wea. Rev.* **113**, 1499-1509.

McBride, J. L., and R. Zehr, 1981: Observational analysis of tropical cyclone formation. Part II: Comparison of non-developing versus developing systems. *J. Atmos. Sci*, **38**, 1133-1151.

Palmen, E. H., 1948: On the formation and structure of tropical cyclones. *Geopysica Helenski*, **3**, 26-38.

Ramage, C. S., 1959: Hurricane development. *J. Meteor.*, **16**, 227-237.

Riehl, H., 1948: On the formation of typhoons. *J. Meteor.*, **5**, 247-264.

Rossby, C. G., 1945: On the propagation of frequencies and energy in certain types of oceanic and atmospheric waves. *J. Meteor.*, **2**, 187-204.

# VITA

Vicki Anne Millier [redacted]

She is the second of three children born to Jack and Beverly Millier. She spent her junior year of high school as a foreign exchange student in Goslar, Germany. She returned to the United States and graduated from American High School in Fremont, California in 1977.

Vicki attended San Jose State University from 1977 to 1980 where she studied German. She then transferred to University of California Davis, and obtained a B.S. in Atmospheric Science in 1983.

After entering the U.S. Air Force and attending Officer Training School in 1983, she worked as a Wing Weather Officer at March AFB in Riverside, California. In 1985 she was transferred to Howard AFB, Panama where she worked as a Staff Weather Officer and Meteorological Satellite Coordinator. Included in her regular weather support duties were frequent exercise deployments to locations throughout Central and South America. In 1987 she was selected for an AFIT advanced degree assignment to Texas A&M University.

[redacted]